UNLIMITED
UNCLASSIFIED

ILLIMITÉ
NON CLASSIFIÉ

Technical Report

Rapport technique

1985/05

TR-WE-46
NRC NO. 24967
TDC NO. TP 6939E

ESTABLISHMENT OF QUANTITATIVE WEAR AND FATIGUE MODEL FOR RAILWAY RAIL SUBJECTED TO HEAVY TRAFFIC CONDITIONS AND DIFFERENT LUBRICATION REGIMES

J. Kalousek

Division of
Mechanical Engineering

Division de
génie mécanique

CA1
DTC 845
85
E76
c.2

National Research Council Canada
Conseil national de recherches Canada

Canada

86-0570/

DIVISION OF MECHANICAL ENGINEERING PUBLICATIONS

DM **(Division of Mechanical Engineering Report)**
Scientific and technical information considered important, complete and a lasting contribution to existing knowledge.

TR **(Technical Report)**
Information less broad in scope but a substantial contribution to existing knowledge.

CTR **(Controlled/Classified Technical Report)**
A Technical Report with controlled distribution for national security, proprietary or other reasons.

LM **(Laboratory Memorandum)**
Preliminary or exploratory information with controlled distribution.

CAT **(Calibration Analysis and Test Report)**
Information on minor laboratory projects or services.

PUBLICATIONS DE LA DIVISION DE GÉNIE MÉCANIQUE

DM **(Rapport de la Division de génie mécanique)**
Informations scientifiques et techniques jugées importantes, complètes et susceptibles de contribuer de façon durable à l'avancement des connaissances courantes.

TR **(Rapport technique)**
Informations de moindre importance, mais pouvant contribuer substantiellement à l'avancement des connaissances actuelles.

CTR **(Rapport technique à diffusion contrôlé/classifié)**
Rapport technique à diffusion contrôlée pour des raisons de sécurité nationale, de propriété intellectuelle et autres.

LM **(Mémoire de laboratoire)**
Informations préliminaires ou de nature exploratoire à diffusion contrôlée.

CAT **(Rapport d'étalonnage d'analyse et d'essai)**
Informations sur de petits projets ou des services de laboratoire.

UNLIMITED
UNCLASSIFIED

ILLIMITÉ
NON CLASSIFIÉ

Library and Information Centre
Centre de documentation (GSL)
RECEIVED – REÇU LE
DEC 5 1985
Government Publication Officielle
Transport Canada / Transports Canada

ESTABLISHMENT OF QUANTITATIVE WEAR AND FATIGUE MODEL FOR RAILWAY RAIL SUBJECTED TO HEAVY TRAFFIC CONDITIONS AND DIFFERENT LUBRICATION REGIMES

Progress Report
April 84 to March 85

Submitted by:
J. Kalousek

Sponsor Organizations:

Transport Canada
Transportation Development Centre
Montreal, Canada

and

Association of American Railroads
Technical Research Center
Chicago, U.S.A.

Technical Report

Rapport technique

1985/05

TR-WE-46
NRC NO. 24967
TDC NO. TP 6939E

Dr. C. Dayson, Head/Chef
Western Laboratory/Laboratoire de l'ouest
Vancouver, B.C., Canada
V6R 1P5

Mr. E.H. Dudgeon
Director/
Directeur

REPORT DOCUMENTATION FORM

1. Transport Canada Report No.	2. TDC Project No.	3. Recipient's Catalogue No.
TP 6939E	6155	

4. Title and Subtitle	5. Report Date
Establishment of Quantitative Wear and Fatigue Model for Railway Rail - 1984/85 Progress Report	May 1985
	6. Performing Organization Report No.
7. Author(s)	8. Transport Canada File No.
J. Kalousek, D. Fegredo, H. Ghonem, E.E. Laufer, R.K. Steele	D1465-366-4
9. Performing Organization Name and Address	10. DSS File No.
National Research Council of Canada (NRC) Western Laboratory 3904 West 4th Avenue Vancouver, B.C. V6R 1P5	11. DSS or Transport Canada Contract No. 6155
12. Sponsoring Agency Name and Address	13. Type of Report and Period Covered
Transportation Development Centre (TDC) Guy Complex Favreau 200 Dorchester Blvd. West Suite 601, West Tower Montreal, Que. H2Z 1X4	Technical April 84-March 85
	14. Sponsoring Agency Code TDC 6155
15. Supplementary Notes	16. TDC Project Officer
This is a cooperative project between the Transportation Development Centre and the Association of American Railroads.	D.W. Dibble

17. Abstract

The research objective of the wear and fatigue model is to identify the theoretical and practical measures aimed at the extension of rail life. The research efforts, carried out jointly by the National Research Council (NRC) of Canada and the University of Rhode Island (URI), have concentrated that at the NRC, on studies of mechanical, metallurgical and rheological parameters influence the wear and contact fatigue processes; while the URI has set out to determine the basic fatigue properties of rail steels in a compressive, biaxial stress environment.

This report is concerned with segments of the overall research program completed at NRC during the 1984/85 contract period and consists of a collection of two papers and one report. The first paper deals with the wear rate and fatigue crack initiation and growth measurements carried out on several commercial and experimental pearlitic rail steels. The second paper is concerned with the wear and contact fatigue properties of pearlitic, bainitic and tempered martensite steels at hardness levels of HRC 38, 42 and 45. The findings of an electron microscope study of the white etching phase, found in rail wear debris and on the rail surface, forms the final portion of this report.

18. Key Words	19. Distribution Statement
Rail Life, Wear, Lubrication and Metallurgy	Limited number of copies available from TDC

20. Security Classification (of this report)	21. Security Classification (of this page)	22. No. of Pages	23. Price
Unclassified	Unclassified		---

TDC CDT 79-005

FORMULE DE DOCUMENTATION POUR RAPPORT

1. N° du rapport Transports Canada	2. N° de l'étude — CDT	3. N° de catalogue du destinataire
TP 6939E	6155	

4. Titre et sous-titre	5. Date du rapport
Establishment of Quantitative Wear and Fatigue Model for Railway Rail - 1984/85 Progress Report	mai 1985
	6. N° du rapport de l'organisme exécutant

7. Auteur(s)	8. N° de dossier Transports Canada
J. Kalousek, D. Fegredo, H. Ghonem, E.E. Laufer, R.G. Steele	D1465-366-4

9. Nom et adresse de l'organisme exécutant	10. N° de dossier — ASC
Conseil national de recherches Canada Laboratoire de l'ouest 3904 ouest, 4ième avenue Vancouver, B.C. V6R 1P5	11. N° de contrat — ASC ou Transports Canada 6155

12. Nom et adresse de l'organisme parrain	13. Genre de rapport et période visée
Centre de dévloppement des transports (CDT) Complexe Guy Favreau 200 ouest, boul. Dorchester Suite 601, tour ouest Montreal, Que. H2Z 1X4	Technique; avril 84-mars 85
	14. Code de l'organisme parrain CDT 6155

15. Remarques additionnelles	16. Agent de projet — CDT
Ceci est un programme de recherche conjoint, parrainé par le Centre de développement des transports et Association of American Railroads	D.W. Dibble

17. Résumé

Ce rapport décrit la recherche concernant le modèle mathématique figurant les paramètres en jeu dans le processus d'usure et de fatigue des rails de chemins de fer et visant à trouver des méthodes permettant de prolonger la vie de ces rails. Ce programme de recherche a été lancé conjointement par le Conseil national de recherches du Canada (CNR) et l'université de Rhode Island aux Etats-Unis. Les travaux du CNR ont porté sur les paramètres mécaniques, métallurgiques et rhéologiques qui ont une influence sur les processus d'usure et de fatigue par contact, tandis qu'à l'université Rhode Island, on a cherché à déterminer la tenue à la fatigue des aciers pour rails et leur comportement sous contraintes biaxiales en compression.

Il présente les travaux effectués par le CNR durant l'exercise 1984-1985 et consignés dans deux communications et un rapport de recherche. La première communication concerne les essais visant à déterminer la tenue à l'usure et à la fatigue de contact de plusieurs aciers perlitiques pour rails, commerciaux ou expérimentaux; la deuxième traite des propriétés des aciers perlitique, bainitique et martensitique revenu, ayant une dureté de 38, 42 et 45 HRC, respectivement. Pour terminer, il décrit les résultats de l'examen au microscope électronique à balayage en transmission sur les particules correspondant aux zones blanches trouvées à la surface des rails ou résultant de l'usure de ceux-ci.

18. Mots-clés	19. Diffusion
Vie des rails, usure, lubrification, métallurgie.	Le Centre de développement des transports dispose d'un nombre limité d'exemplaires

20. Classification de sécurité (de ce rapport)	21. Classification de sécurité (de cette page)	22. Nombre de pages	23. Prix
non-classifié	non-classifiée		---

ACKNOWLEDGEMENT

The financial support provided by the Transportation Development Centre (Canada) and the Association of American Railroads, towards the research projects described in this report, is most gratefully acknowledged.

ABSTRACT

This is the third annual progress report concerned with the research program jointly being carried out at the National Research Council of Canada (NRCC) and the University of Rhode Island (URI), USA. The program strives for the development of a wear and fatigue model of railway rail which, by identifying the relationships between relevant variables, aims at identification of practical measures to extend the rail life. Indeed, the laboratory and field tests combined with theoretical analysis carried out during the course of our investigations strongly suggests that significant increase in rail life could be obtained by specific combinations of lubrication and grinding practices, the former taking care of gauge side wear and the latter alleviating, or even preventing, the occurrence of contact fatigue.

Though the complete report on our model will not be available until March 1986, this progress report consists of two previously published papers containing some partial results obtained at the NRC - Western Laboratory and one report describing the transmission electron microscope (TEM) investigation of the white etching layer which was subcontracted to the Technical University of Nova Scotia. The progress accomplished in the area of initiation and propagation of contact fatigue cracks in rail steels is reported separately in the form of a Master of Science Thesis entitled, "Design of a Biaxial Fatigue Loading System to Simulate Rolling Contact Process". A copy of this thesis, submitted to the URI in April 1985 by Samuel Kumar may be obtained by writing to the University library or Professor H. Ghonem, Dept. of Mechanical Engineering, URI, Kingston, Rhode Island, 02881, USA.

The first paper is concerned with the wear and contact fatigue evaluation of several commercial and experimental rail steels. The 70 mm diameter test discs were subject to 2.4 million revolutions in the one tenth scale rail/wheel wear apparatus which simulated the interaction between a freight car wheelset and pair of rails in a 235 m radius (8°) curve. The wear rates were established for dry, grease and sand contaminated grease lubrication regimes. Lubrication reduced the wear rates by up to two orders of magnitude, with the largest reduction observed in the case of plain carbon rail. Upon completion of the test the discs were sectioned and metallographically examined to establish the extent of fatigue cracks. The results show that the steels with improved dry wear resistance do not necessarily exhibit the same degree of improvement to fatigue damage.

The second paper desribes our efforts to find out if it is worthwhile to produce premium rail steels harder than HRC 36 to HRC 39 (≈ 335 to 365 BHN) and to discover the best microstructure for wear resistant rail. Thus, an experimental Cr-Mo alloy rail steel was heat treated to pearlite, bainite and tempered martensite at hardness levels of HRC 38, 42 and 45 (≈ BHN 360, 390, 420). The discs were subject to the same test sequence and lubrication environments described in the first paper. Dry wear rates decreased significantly with increasing hardness in high rail discs with tempered martensite or bainite microstructures, but were almost independent of hardness for pearlite

in the range tested. It is concluded that pearlite gives the best dry wear performance, and there is no advantage in increasing hardness beyond HRC 38-40 (≈ BHN 355 to 370). The superior performance of pearlite in dry wear appears to be due to a very pronounced work hardening near the wearing surface. In the lubricated regime the pearlite also showed fewer contact fatigue cracks than tempered martensite.

The Technical University of Nova Scotia report describes an optical and transmission electron microscope investigation of a number of large flakes (mm to cm) to identify the "white etching" constituent of their microstructures. The earlier investigation (see 1983/84 progress report) of small (μm - mm) wear particles collected from tangent track rail showed that many white etching particles were, in fact, a fine mechanical mixture of sand and steel. In this investigation, however, the microstructures observed were similar to those seen in the worn rail consisting of fine work hardened pearlite. In most cases the white etching constituent was a pearlite with very fine, though broken up, cementite lamellae which was more resistant to etching than coarser pearlite. One of the white etching regions was identified as tempered martensite. No regions of untempered martensite or massive cementite were found.

RÉSUMÉ

Troisième rapport annuel sur l'état d'avancement du programme de recherche conjoint lancé par le Conseil national de recherches du Canada (CNR) et l'université Rhode Island des Etats-Unis, ce rapport concerne l'élaboration d'un modèle mathématique figurant le processus d'usure et de fatique des rails. Par ce modèle, on vise à établir des corrélations entre les différentes variables prises en compte dans le but de mettre au point des méthodes permettant de prolonger la vie des rails. Effectivement, les essais de laboratoire et in situ, conjugués aux études analytiques faisant partie du programme de recherche, laissent croire qu'il est possible de prolonger sensiblement la vie utile des rails par les procédés combinés de lubrification et de meulage, la première pour réduire l'usure latérale et le deuxième pour atténuer, voire éliminer, l'usure due à la fatigue de contact.

Il est entendu que le rapport final sur le modèle mathématique ne pourra paraître avant mars 1986. Entre-temps, nous soumettons le présent rapport d'avancement qui comprend les deux communications précédemment publiées et renfermant les résultats partiels obtenus de la recherche menée par le CNR dans ses laboratoires de l'Ouest, ainsi que le rapport sur l'examen au microscope électronique à balayage en transmission sur les particules correspondant aux zones blanches, lequel avait été sous-traité à la Technical University of Nova Scotia. Quant à la recherche concernant l'apparition et la propagation de fissures dues à la fatigue de contact, elle a fait l'objet d'une thèse de maîtrise intitulée "Design of a Biaxial Fatigue Loading System to Simulate Rolling Contact Process" que son auteur, Samuel Kumar, a soutenue en avril 1985. Pour obtenir un exemplaire de cette thèse, s'addresser par écrit à la bibliothèque de l'université de Rhode Island ou bien au professeur H. Ghonem, Department of Mechanical Engineering, University of Rhode Island, Kingston, Rhode Island 02881, U.S.A.

La première des deux communications traite des essais visant à déterminer la tenue à l'usure et à la fatigue de contact de plusieurs rails, commerciaux et expérimentaux. Ces essais ont été faits à l'aide d'éprouvettes disques de 70 mm de diamètre qui ont subi 2,4 millions révolutions sur l'appareil au $1/10^e$ destiné à mesurer l'usure de contact roues-rails, grâce auquel on a simulé l'interaction entre un essieu monté de wagon de marchandises et une voie en courbe ayant un rayon de 235 m (8 degrés de courbure).

Il s'agissait d'établir les taux d'usure sous divers régimes de contact: contact sec, contact lubrifié et contact lubrifié contaminé de sable. Par la lubrification, les taux d'usure ont pu être réduits par quelque deux ordres de grandeur, notamment dans le cas du rail acier au carbone classique. Une fois les essais terminés, les éprouvettes ont été sectionnées et soumises à un examen métallographique destiné à déterminer l'étendue des fissures. Ces examens ont montré qu'une amélioration dans la résistance des aciers à l'usure à sec n'apporte pas nécessairement une amélioration de même degré dans la tenue à la fatigue de contact.

La deuxième communication décrit les essais faits pour déterminer l'utilité de réaliser des aciers pour rails d'une dureté supérieure à la gamme 36-39 HRC (équivalent à 335-365 BHN), et pour trouver la microstructure idéale d'un acier résistant à l'usure. C'est ainsi que par traitement thermique il a été donné à un acier au cr-mo une structure perlitique, bainitique et de martensite

revenue correspondant à des duretés de 38, 42 et 45 HRC, respectivement (équivalent à des duretés 360, 390 et 420 BHN). Quant au mode opératoire et aux régimes de contact, ils ont été les mêmes que pour les essais décrits dans la première communication. Il a été constaté que les taux d'usure en contact sec diminuent sensiblement à mesure que les duretés augmentent pour les aciers des rails de la file extérieure ayant une structure bainitique ou de martensite revenue, mais que ces taux devenaient insensibles à la dureté dans le cas d'une structure perlitique, du moins dans la gamme des duretés prises en compte. La conclusion a été que la perlite donne la meilleure tenue en contact sec et qu'il n'y aurait aucun avantage à réaliser des aciers d'une dureté supérieure à la gamme 38-40 HRC (équivalent à 355-370 BHN). La meilleure performance de la perlite en contact sec serait attribuable à un écrouissage prononcé dans le voisinage de la surface d'usure. En régime de contact lubrifié, elle a également montré un nombre de fissures superficielles plus faible que dans le cas de la martensite revenue.

Le rapport établi par la Technical University of Nova Scotia décrit la recherche faite à l'aide du microscope électronique à balayage en transmission sur des échantillons d'une grosseur allant du millimétrique au centimétrique, dans le but de découvrir la composition des particules correspondant aux zones blanches. Précédemment (voir le rapport d'avancement 1983/1984) la recherche avait porté sur des particules d'une grosseur allant du micrométrique au millimétrique, prélevées sur un rail de voie courbe, et elle avait montré que plusieurs de ces particules résultaient en réalité d'un mélange extrêmement fin de sable et d'acier. Dans la présente recherche, cependant, les microstructures observées ressemblaient à celles du rail usé, c'est-à-dire une structure perlitique fine écrouie. Dans la plupart des cas, les zones blanches observées étaient faites de perlite comportant de la cémentite en lamelles très fines quoique décomposées, qui rendent celle-ci plus résistante qu'une perlite plus grossière. Une des zones blanches a été reconnue comme étant de la martensite revenue. Aucune zone de martensite non revenue ou de cémentite grossière n'a été observée.

CONTENTS

		Page
	REPORT DOCUMENTATION PAGE (TDC)	(i)
	FORMULE DE DOCUMENT POUR RAPPORT (TDC)	(ii)
	ACKNOWLEDGEMENT	(iii)
	ABSTRACT	(iv)
	RÉSUMÉ	(v)
PART I:	**WEAR AND LUBRICATION EFFECT ON SUBSURFACE FAILURE OF SEVERAL STEELS**	
1.0	INTRODUCTION	1-1
2.0	EXPERIMENTAL INVESTIGATIONS	1-2
	2.1 Test Apparatus	1-2
	2.2 Materials Tested	1-3
	2.3 Test Procedures	1-4
3.0	EXPERIMENTAL RESULTS AND DISCUSSION	1-5
	3.1 Wear Rates	1-5
	3.1.1 Dry wear	1-5
	3.1.2 Material removal under lubricated conditions	1-6
	3.2 Statistical Analysis of Crack Measurements	1-7
4.0	QUALITATIVE MODELLING OF CONTACT FATIGUE	1-9
	4.1 Stress Strain Cycles and Associated Fatigue Mechanisms in Surface and Subsurface Layers	1-9
5.0	CONCLUDING REMARKS	1-11
6.0	REFERENCES	1-11
	REPORT DOCUMENTATION PAGE (NRC)	

CONTENTS Cont.

PART I: LIST OF ILLUSTRATIONS

Figure		Page
1	(a) Dry gauge face wear on outer rail (side cutting) (b) Flaking and spalling on the inner rail	1-13 1-13
2	Schematics of Rail Wheel Wear Test Apparatus	1-14
3	Rate of material removal at (a) no lubrication; (b) grease sand and (c) grease only lubrication	1-15
4	New and worn profiles of inner and outer rail discs (a) Specimens A; (b) Specimens I	1-16
5	Wear debris (a) no lubrication - outer rail disc A; (b) no lubrication - outer rail disc I; (c) grease-sand lubrication - outer rail disc I; (d) grease only lubrication - outer rail disc A	1-17
6	Schematics of contact fatigue damage on the outer rail or rail disc	1-18
7	Cross section at a gauge corner of outer rail disc Specimen G	1-19
8	Streses due to (a) normal and (b) tangential loads	1-20
9	Shear stress distribution and associated stress-cycle at (a) immediate surface layer; (b) subsurface surface layer; (c) deep subsurface layer	1-21
10	Contact fatigue damage of (a) top surface of inner rail disc A and (b) gauge corner of outer rail disc E	1-22
11	(a) Schematics of flake initiation, growth and release mechanism and (b) An example of flake before its release at the gauge corner of outer rail disc I	1-23

PART I: LIST OF TABLES

Table		
1	Materials Tested	1-3
2	Summary of statistical analysis	1-8

CONTENTS Cont.

PART II: THE WEAR RESISTANCE AND WORN METALLOGRAPHY OF PEARLITE, BAINITE AND TEMPERED MARTENSITE RAIL STEEL MICROSTRUCTURES OF HIGH HARDNESS

		Page
1.0	INTRODUCTION	2-1
2.0	EXPERIMENTAL PROCEDURE	2-1
	2.1 Test Rig	2-1
	2.2 Materials	2-2
	2.3 Wear Tests	2-2
	2.4 Metallography	2-4
3.0	OBSERVATIONS	2-4
	3.1 Wear Tests	2-4
	3.1.1 Wear rates	2-4
	3.1.2 Wear profiles	2-5
	3.2 Metallography	2-5
	3.2.1 Optical and SEM	2-5
	3.2.2 Microhardness measurements	2-7
	3.2.3 TEM	2-7
4.0	DISCUSSION	2-9
5.0	SUMMARY AND CONCLUSIONS	2-12
6.0	REFERENCES	2-12

PART II: LIST OF TABLES

Table

1	Summary of Materials and Test Sequences	2-16
2	Approximate depth (μm) of grossly deformed shear zone in high rails from the worn surface to where the grains become just recognisable	2-17
3	Hardness (HV_{100}) at various depths (μm) below the worn surface for low rail discs	2-18

PART II: LIST OF ILLUSTRATIONS

Figure		Page
1	Wear rates observed: (a) no lubrication; (b) grease/ 20% sand lubrication; (c) pure grease lubrication.	2-19
2	Wear profiles after each of the four test stages: (a) disks A, tempered martensite; (b) disks D, bainite; (c) disks G, pearlite	2-20
3	Gauge corner and gauge face wear after two periods of dry wear resulting in development of shoulder (a) or shear lip (b): (a) disk K-HR, tempered martensite; (b) disk J-HR, pearlite	2-21
4	Gauge corner deformation with surface and subsurface cracks: (a) disk K-HR; (b) disk A-HR; (c) disk J-HR; (d) disk G-HR	2-22
5	Crack frequency vs length, image analyser data	2-23
6	Association of cracks with inclusions: (a) disk K-HR, MnS inclusions; (b) disk J-HR, MnS inclusions; (c) disk A-HR, undeformed oxide inclusions	2-24
7	Undeformed microstructures: (a) tempered martensite (disk K-HR); (b) pearlite (disk G-HR); (c) bainite (disk D-HR)	2-25
8	Worn near-surface microstructure: (a) disk K-HR, tempered martensite, dry wear; (b) disk J-HR, pearlite dry wear; (c) disk A-HR, tempered martensite, full sequence; (d) disk G-HR, pearlite, full sequence; (e) disk D-HR, bainite, full sequence	2-26
9	Typical microhardness traverses at the centre of: (a) running surface; (b) gauge corner; (c) gauge face	2-27
10	Gauge corner microhardness traverses, samples J-HR and K-HR.	2-32
11	(a) Disk H-HR, 30 μm below running surface. TEM, Thinned foil; (b) diffraction pattern corresponding to (a)	2-28
12	Disk E-HR, between gauge corner and centre of running surface. TEM, thinned foil, (a) bright field; (b) dark field {110} reflection; (c) diffraction pattern	2-29
13	(a) Disk A-HR, 70 μm below running surface. TEM, thinned foil. (b) Diffraction pattern corresponding to (a)	2-30
14	Two stage carbon replica, TEM; Disk J-HR (a) gauge surface, (b) 50 μm and (c) 500 μm below surface; Disk K-HR (d) gauge corner surface, (e) 50 μm and (f) 500 μm below surface	2-31
15	Inter-carbide spacing vs depth below gauge corner surface (J-HR and K-HR)	2-32

CONTENTS Cont.

PART III: EXAMINATION OF RAIL WEAR DEBRIS

		Page
1.0	INTRODUCTION	3-1
2.0	EXPERIMENTAL	3-1
	2.1 Sample Preparation - TEM	3-1
	2.2 Phase Identification	3-1
	2.3 Optical Metallography	3-3
3.0	OBSERVATIONS	3-3
	3.1 Sample K-1	3-3
	3.2 Sample K-3	3-3
	3.3 Sample K-6	3-4
	3.4 Sample K11P	3-4
	3.5 Sample K18P	3-4
	3.6 Sample K21	3-4
	3.7 Sample K40P	3-4
4.0	SUMMARY AND CONCLUSIONS	3-5
5.0	REFERENCES	3-5

PART III: LIST OF ILLUSTRATIONS

Figure		
1	Macro Photo of K1 Flake, (Neg. 31B)	3-6
2	Optical Micrograph of K1 Flake, 1,000 × (Neg. 26KF)	3-6
3	(a) Sample K1, 75,000 × (Neg. 3294)	3-7
	(b) Diffraction Pattern Corresponding to Figure 3(a), (Neg. 3295)	3-7
4	(a) Sample K1, 25,000 × (Neg. 3296)	3-8
	(b) Diffraction Pattern Corresponding to Figure 4(a) (Neg. 3297)	3-8
5	Macro Photos of K3 Flake (Neg. 20D)	3-9

Figure		Page
6	Optical Micrograph of K3 Flake, 500 × (Neg. 17KF)	3-9
7	(a) Sample K3, 25,000 × (Neg. 3367)	3-10
	(b) Diffraction Pattern Corresponding to Figure 7(a) (Neg. 3368)	3-10
	(c) Dark Field, same area as 7(a), 110 Reflection, 25,000 × (Neg. 3369)	3-11
8	Macro Photo of K6 Flake (Neg. 26D)	3-12
9	Optical Micrograph, 500 × (Neg. 6KF)	3-12
10	(a) Sample K6, 25,000 × (Neg. 3352)	3-13
	(b) Diffraction Pattern Corresponding to Figure 10(a) (Neg. 3353)	3-13
11	Macro Photo of K11P Flake (Neg. 35C)	3-14
12	Optical Micrograph of K11P Flake, 500 × (Neg. 4KF)	3-14
13	Sample K11P, 25,000 × (Neg. 3358)	3-15
14	(a) Sample K11P, 25,000 × (Neg. 3362)	3-16
	(b) Diffraction Pattern Corresponding to Figure 14(a) (Neg. 3363)	3-16
15	Macro Photo of K18P Flake (Neg. 4C)	3-17
16	Optical Micrograph of K18P Flake, 1,000 × (Neg. 50KF)	3-17
17	(a) Sample K18P, 6,000 × (Neg. 3242)	3-18
	(b) Diffraction Pattern Corresponding to Figure 17(a) (Neg. 3244)	3-18
	(c) Dark Etching Region, same as 17(a), 75,000 × (Neg. 3245)	3-19
18	Macro Photo of K21 Flake (Neg. 7c)	3-20
19	Optical Micrograph of K21 Flake, 500 × (Neg. × 12KF)	3-20
20	Sample K21, 75,000 × (Neg. 3343)	3-21
21	(a) Sample K21, Another Area, 75,000 × (Neg. 3344)	3-22
	(b) Diffraction Pattern Corresponding to Figure 21(a) (Neg. 3345)	3-22
22	Sample K21, 25,000 × (Neg. 3347)	3-23
23	Optical Micrograph of K40P Flake, 500 × (Neg. 23KF)	3-24

Figure		Page
24	Optical Micrograph of K40P Flake, Another Area, 500 × (Neg. 24KF)	3-24
25	(a) Sample K40P, 75,000 × (Neg. 3156)	3-25
	(b) Diffraction Pattern Corresponding to Figure 25(a) (Neg. 3153)	3-25
26	(a) Sample K40P, Another Area, 75,000 × (Neg. 3157)	3-26
	(b) Diffraction Pattern Corresponding to Figure 26(a) (Neg. 3158)	3-26

PART III: LIST OF TABLES

Table		
1	Expected Diffraction Pattern	3-2

PART I

WEAR AND LUBRICATION EFFECT ON SUBSURFACE FAILURE OF SEVERAL STEELS

WEAR AND LUBRICATION EFFECT ON SUBSURFACE FAILURE OF SEVERAL STEELS

1.0 INTRODUCTION

Wear and fatigue damage of rail steels costs North American Railways hundreds of millions of dollars annually [Ref. 1]. Most of this damage occurs on main line track carrying traffic densities greater than 9.0 million gross tonnes annually. Approximately one third of main line maintenance costs are spent on replacement of worn or damaged rails in curves, which only represents 8% or less of main line trackage. The desire to reduce these costs is a powerful incentive for studying the rail/wheel interaction phenomena theoretically and experimentally, both full-scale and in the laboratory.

The rails are removed from curves either due to severe adhesive wear, or fatigue damage of the surface and subsurface layers of the railhead. An example of adhesive wear on the outer, and fatigue damage on the inner, rails is shown respectively in Figures 1(a) and (b). To prevent severe adhesive wear or side cutting in curves, North American railways introduced lubrication and premium rails. Although dry wear may occur intermittently on rails in curves due to the failure of the lubrication equipment, for the most part, the rails remain well lubricated.

Laboratory investigations of the dry wear occurring between the wheel flange and the side of the railhead have been carried out during the past decade by numerous authors. Beagley [Ref. 2] and Bolton and Clayton [Ref. 3], studied the side cutting wear processes using rolling-longitudinal sliding contacts produced by a twin disc, Amsler wear testing machine. Beagley established the transition between mild and severe wear for BS11 and 1% chromium steels as a function of maximum hertzian pressure, p_o, in the range of 400 to 1,600 MN/m^2, and a longitudinal creepage in the range of 0 to 6%. Bolton and Clayton, however, pointed out that the successful simulation of gauge face wear on the Amsler machine requires a longitudinal creepage of 10 to 35% and p_o = 1,300 MN/m^2. This simulation of side cutting proved more successful because the periferal speed difference between the Amsler specimens approached that by which flange asperities strike the side of rail [Ref. 4].

Johns and his co-workers [Ref. 5] illustrated the possible contact stress patterns between running surfaces of worn rails and treads of worn wheels for a wheelset laterally offset from its central position and subject to several load levels. For the centrally located wheelset loaded by 30 tonnes, Johns and his co-workers calculated that p_o = 830 MN/m^2 at both inner and outer rail contact areas. The same load yielded a p_o in the range of 1,500 to 3,000 MN/m^2 when the wheelset was offset by 1 to 2.5 cm on either side. These contact stress increases were caused by changes in contact geometry which, for example, occur between the flange root and gauge corner of outer rail, or between the 'false flange' and field side of inner rail. Furthermore, using a computer algorithm, they demonstrated the effect of transverse tractions in the rail/wheel interface on hertzian contact stresses. The stress

component most affected by transverse tractions is the maximum transverse stress which at all times occurs at the surface. Its value increases by 64% to 106% when the ratio of tractive to normal force, T/N, increases from 0.3 to 0.5, respectively. These levels of contact stresses exceed the shakedown limit and pronouncedly affect the development of contact fatigue damage of any commercially produced pearlitic rail steels.

Numerous studies concerned with contact fatigue of ball or roller bearings, gears, and traction drives have been carried out. In order to apply the information derived from these studies to a specific rail/wheel tribosystem, the development of both theoretical and experimental investigation of damage mechanism in rails is clearly desirable. It is essential that the traction and normal forces, contact stresses, lubrication environment and metallurgical parameters used in such studies match as closely as possible those occurring in the field.

2.0 EXPERIMENTAL INVESTIGATIONS

2.1 Test Apparatus

The tests were carried out on a four disc wear apparatus which was designed to simulate the interaction between a railway wheelset and pair of rails. The rail discs were 69.9 mm in diameter. A numerically controlled lathe was used to machine a new 136 lb/yard AREA profile onto the crown of each rail disc. The wheel discs were 120.7 mm in diameter at the center of the tread, and machined to a worn wheel profile designated 'CN profile A'. Both rail and wheel profiles were reduced ten times in their cross sections.

As shown in Figure 2, the wheel discs were rigidly mounted to a shaft and represented a wheelset. This wheelset could be misaligned with respect to the rail discs by rotating the rear support of the flexure pivot assembly around the vertical axis of the wheelset. Such misalignment, termed 'angle of attack' or 'yaw angle', produces traction force in a transverse direction. The lateral softness of the flexure pivots enabled the transverse traction forces to move the wheelset into flange contact.

The load was applied to the centre of the wheelset by a dead weight lever system equipped with another set of flexure pivots, which were designed to minimize the effect of applied load on the measurement of transverse and spin components of rail/wheel disc traction forces. This ensured that the occurrence of flanging was the function of yaw misalignment, geometry of disc profiles, and contamination, but independent of the wheelset loading system. The orthogonal components of a load vector transmitted between the right and left-hand parts of the rail and wheel discs were measured by loadcells. The rail discs were driven by a 14.7 kw, reversible and variable speed DC motor. The unrestrained rolling of the wheelset ensured the modelling of the interactions between the freight car wheelset rather than the locomotive and track.

The repeatability of test procedures was ensured by microprocessor controlled activation of the motor, yaw angle, and lubrication devices. The microprocessor was also used to periodically record the revolution counts, distribution of rail/wheel forces, and the history of longitudinal and lateral creepages during the test.

2.2 Materials Tested

Table 1 identifies the steel type, chemical composition and hardness of tested discs. All discs, with the exception of G and H, were manufactured from the heads of as rolled, commercially available rails. The G discs were machined from commercially cast nodular iron railway wheel. This material may be considered for the track sections which could be cast, such as switch points and frogs. The H discs were machined from laboratory heat of pearlitic steel, the ferrite matrix of which contained vanadium nitrides.

Table 1: Materials tested

CODE	RAIL TYPE	C	Mn	Si	Cr	OTHERS	VHN
A	Standard AREA	.80	.90	.20			260
B	Cr alloyed	.75	.65	.25	1.2		320
C	Cr-Mo alloyed	.65	.95	.30	.65	Mo = .16	330
D	Through hardened	.75	.90	.30			340
E	Cr-Si-Cb alloyed	.70	1.1	.55	.80	Cb = .06	340
F	Through hardened	.80	.90	.20			370
G	Nodular iron	3.3	.66	2.5		Mo = .28, Cu = .73	330
H	Cr-V alloyed	.80	.95	.30	1.2	V = .3 N = .017	370
I	Head hardened	.65	.90	.20			370

2.3 Test Procedures

Two discs from each metallurgy, one experiencing outer, and the other inner, rail loading environment were subject to sixty periods of 40,000 revolutions. To simulate the intermittent occurrence of dry wear in curves, the lubrication of discs was changed during the length of each test in the following manner:

Step 1: The first period of 40,000 revolutions was run dry at an ambient temperature of 19°C and relative humidity of 45%. The disc surfaces were cooled by blowing air. This air stream also transported the loose wear particles from the wearing surface to the nearby magnets.

Step 2: The next nineteen periods (760,000 revs.) were lubricated by a calcium soap based grease mixed with 20% quartz sand. The grease contained a mineral oil with a viscosity of $0.02 Ns/m^2$ (at the atmospheric pressure), and the following EP additives: 11% graphite and 2.5% molybdenum disulphide. The sand, regardless of its initial grain size, was crushed into particles ranging in size from .5 to 5 μm. The grease-sand paste which formed in the interface yielded a boundary lubrication regime and a coefficient of adhesion of .18. This lubrication regime is the most typical of those field conditions where the grease is dispersed to prevent side cutting, and where sand is thrown in by the locomotives to increase traction.

Step 3: Same as Step 1.

Step 4: The remaining 39 periods (1.56×10^6 revs.) were lubricated by the same grease used in Step 2, but without any sand. The contamination of grease by wear particles could not be prevented, thus producing a boundary lubrication regime with the limiting coefficient of friction in the range of .09 to .12. The grease only lubrication, though less realistic in terms of field conditions than lubrication by a grease-sand mixture, was used to enhance the rate of contact fatigue damage to rail discs.

The wheelset load during all tests was 7,000 N. It produced p_o = 1,800 MPa between the inner and outer rail/wheel discs for the case of centrally located wheelset, and p_o = 2,500 MPa between outer rail/wheel discs for laterally displaced wheelset. These contact stresses are in the range reported by Johns et al [Ref. 5] for the field conditions.

Within each period the yaw angle was alternated each 2,500 revolutions between 10', 18', 36' and 40' of arc. These four values represent the mean yaw angles measured on the trailing and leading axles of trailing and leading freight car trucks in a 235 m radius (8°) curve [Ref. 6]. The distribution of forces between the inner and outer pair of discs and the maps of slip vectors in rail/wheel contact as the

function of the above individual angles of attack are described in Reference 7. Each 20,000 revs. the apparatus was stopped, the direction of disc rotation reversed, and the yaw angles changed from a positive to a negative value to maintain the same orientation of curvature.

These test conditions subject the rail disc to an equivalent of 51 million gross tonnes (60 MGT in U.S. customary units) of traffic experienced by rails laid in 235 m radius (8°) curve located in a single main line track, subjected to intermittently changing lubrication regimes and experiencing heavy axle loads in both directions.

Wear was measured by removing both rail discs periodically and weighing them with an accuracy of .05%. At the same intervals the disc profiles were taken with the accuracy of ± 2 μm using an electronic profilometer. The wear debris was collected at the end of each step, and upon completion of the test the specimens were prepared for metallographical examination.

3.0 EXPERIMENTAL RESULTS AND DISCUSSION

3.1 Wear Rates

The rates at which the material was removed from the inner and outer discs during dry, grease-sand and grease only lubrication are shown in Figure 3. Lubrication by grease-sand mixture reduces the material removal 20 times or more, and grease lubrication about 200 times when compared with dry wear.

3.1.1 Dry wear

Figure 4 shows the profiles of inner and outer rail discs A and I taken before and at the end of each step. The A specimen exhibits the larger amount of side cutting and plastic flow. The direction of plastic flow follows the direction of the transverse traction forces, which are towards the field side on the inner disc, and towards the gauge side on the outer disc. While the displaced metal on the inner disc remains undisturbed, on the outer disc it is worn away. In hard pearlitic steels this flow, combined with low wear rates, reduces side cutting as shown in Figure 4(b).

The examination of wear particles, when compared with findings of other researchers [Refs. 2,3] has shown that the inner rail/wheel surfaces have experienced mild adhesive wear. On the other hand, the debris collected from outer rail shows particles up to 2 mm across, in the case of specimen A [Fig. 5a], and up to .75 mm across, in the case of specimen I [Fig. 5b], both of which are representative of severe adhesive wear. The latter particles were formed in a flange contact situation where gross-sliding and self-cleaning of wearing surfaces prevailed.

Assuming that the wear on the top surfaces of inner and outer rail discs was the same, the differential in wear rates between the right and left columns in Figure 3(a) could be attributed to gauge face wear. Steele and Reiff [Ref. 8] proposed that gauge face wear

resistance could be most conviently compared with the Figure of Merit (FM):

$$FM = \frac{\text{average wear rate of standard rail}}{\text{average wear rate of comparison rail}}$$

FM values for the materials tested on the rail/wheel wear apparatus and on a full-scale testing system [Ref. 8] under nonlubricated wear regimes in the gauge face area are as follows:

Wear apparatus: 235 m radius (8°) curve

$$I : F : A \approx 5.3 : 3.5 : 1$$

Full-scale system (coding as per Reference 8):

470 m radius (4°) curve

$$HH : FHT : Std. \approx 3.5 : 2.1 : 1$$

Because the method of measuring wear rates differed between the full-scale system and our apparatus, the former utilizing caliper gauges and the latter specimen weighing, the wear rates for the same steel increased nonlinearly with curvature. Comparison of wear rates was accomplished by prorating one set of the figures of merit. Assuming that the simulated 235 m radius (8°) curve on the wear apparatus increased the FM, with respect to the 470 m (4°) curve at the full-scale system, by a factor of 1.6, then the equivalent FM for a 470 m radius (4°) curve on the wear apparatus becomes prorated to:

470 m radius (4°) curve:

$$I : F : A \approx 3.31 : 2.18 : 1$$

These figures indicate that the simulation of dry wear on the rail/wheel wear apparatus compares favourably with the controlled full-scale environment.

3.1.2 Material removal under lubricated conditions

During grease-sand lubrication the sand grains are crushed into microscopic particles less than 5 μm in size. These particles randomly imbed either into the rail or wheel material and abrade the other. Thus as seen in Figure 3(b), either low or high rail disc would wear more depending on the random manner by which the sand was distributed throughout the rail/wheel disc interfaces. This mild form of abrasive wear was accompanied by the formation of a white etching layer and delamination wear, as discussed in Reference 7. The implication of this portion of the test to the field conditions is that in lubricated territories where the lack of adhesion has to be enhanced by sanding, the rate of material removal is low and unaffected by the hardness or quality of the rail steel. However, the hardness of rail material still affects the resistance to plastic flow. Also, if a

breakdown of lubrication film occurs in the field, the wear rates shown in Figure 3(a), being one order of magnitude larger, will override those generated during lubrication by grease-sand-wear debris mixtures.

During the grease lubrication run, the volume and weight of most of the flakes released from the surfaces of outer and inner rail discs, an example of which is shown in Figure 5(d), were at least 1,000 times heavier than the weight losses per cycle indicated in Figure 3(c). These flakes, which varied considerably in size and thickness, represented the final stage of the contact fatigue process. They were characterized by subsurface and surface initiation and propagation of fatigue cracks, primarily within, and occasionally beyond, the zone of plastically deformed material. The release of these flakes occurred by brittle fracture, as schematically indicated in Figure 6, and the cavity left behind appeared as a shelly spot or spall. We have, firstly, attempted to statistically analyze the extent of cracking on all of the tested steels, and secondly, proposed a qualitative modelling of a mechanism leading to the development of these cracks.

3.2 Statistical Analysis of Crack Measurements

Three rail disc cross sections, taken equidistantly along the circumference of each disc, were polished, etched and examined for cracks under an optical microscope. The lengths of individual cracks were measured. Though we could not determine which cracks were surface, void, or inclusion initiated, we made an assumption that all surface cracks shorter than 60 μm were crack initiation sites. We also noted that cracks larger than 600 μm reached the boundary between the plastically deformed layer and the underlying undeformed steel. Since these cracks can generate 'deep' shells, and the discs (or rails) would be condemned immediately after the release of such shells, we considered these cracks to have a larger damage potential than those which remained confined to the plastically deformed layer. We have also noted the frequency and mean length of all subsurface cracks, an example of which is shown in Figure 11(b). An inclusion was observed at the center of many of these cracks. The crack frequency and average length, in brackets, for all crack categories is shown in Table 2 [p. 1-8]. This table shows again the base hardness of tested steels and the maximum depth of the plastically deformed layer measured at the gauge corner of an outer disc and the field side of an inner disc.

Review of Table 2 shows that the G discs had, with respect to all other discs, a distinctly superior resistance to contact fatigue. The microstructure of these discs consisted of a bainitic matrix containing graphite nodules. Though the base hardness of the G discs lay in the mid-range of pearlitic steels, the maximum depth of their plastically deformed layer was only about one third as thick. Both high and low disc specimens showed low counts of short cracks. As shown in Figure 7 the subsurface cracks did not form.

Table 2: Summary of statistical analysis

CODE	DISC	VHN	WHL	SSC	IS	MSC	LSC	SC
A	O	260	480	65(43)	10	20(215)	2(780)	66
	I		300	26(40)	11	20(182)	3(860)	
B	O	320	390	62(33)	14	29(180)	2(1085)	75
	I		150	8(49)	17	13(150)	-	
C	O	330	390	51(39)	9	21(183)	2(1470)	69
	I		150	-	12	25(178)	-	
D	O	340	360	9(58)	13	32(172)	1(1470)	91
	I		140	2(90)	14	31(168)	-	
E	O	340	380	41(45)	36	47(193)	-	126
	I		150	1(30)	14	29(147)	-	
F	O	370	360	69(24)	23	24(189)	1(750)	76
	I		140	21(22)	14	14(161)	-	
G	O	330	90	-	20	16(128)	-	71
	I		50	-	15	19(103)	-	
H	O	370	360	63(31)	14	23(158)	-	69
	I		140	9(37)	14	18(132)	-	
I	O	370	240	70(46)	8	26(208)	2(780)	86
	I		120	-	14	36(159)	-	

O = outer, I = inner

VHN - Vickers hardness number (kg/mm^2)

WHL - max. depth of work hardened layer (µm)

SSC - count and mean length of subsurface cracks

IS - count of surface crack initiation sites
(cracks < 60 µm in length)

MSC and LSC - count and mean length of medium
(60 to 600 µm) and large (> 600 µm) surface cracks

SC - total count of surface cracks

The fatigue resistance of pearlitic steels was more difficult to evaluate. Good correlation was obtained between the base hardness of steel and the maximum depth of the plastically deformed layer. Steel I showed the lowest depth of the plastically deformed layer, but the number and length of observed cracks lay in mid-range of those observed in other steels. However, the shelling was not evident on the disc surfaces. Steel E, on the other hand, exhibited the lowest number of subsurface cracks but it had the largest number of cracks less than 600 μm long. The high incidence of cracks was accompanied by mild shelling, mainly, on the high rail disc. Though the plain carbon steel, A, did not exhibit extensive cracking in a range below 600 μm, it showed the most frequent occurrence of cracks larger than 600 μm and the thickest plastically deformed layer in both high and low rails. Yet, steel D showed the lowest count of subsurface cracks, but the crack count below 600 μm was on the high side and one of the cracks propagated deep into undeformed material.

Though some differences exist between the discs within each fatigue crack category (SSC, IS, MSC, LSC) the above observations indicate that none of the tested pearlitic materials exhibited distinctly improved resistance to contact fatigue damage.

An important step in interpreting the results of this statistical evaluation is the understanding of rolling fatigue mechanisms in the railhead layers and their relation to shear stress-strain cycles acting in these layers. Based on the work of the authors [Ref. 9], a qualitative analysis of such a mechanism under dry and lubrication conditions is briefly described in the next section.

4.0 QUALITATIVE MODELLING OF CONTACT FATIGUE

4.1 Stress Strain Cycles and Associated Fatigue Mechanisms in Surface and Subsurface Layers

Using the work of Smith and Liu [Ref. 10] and assuming the magnitude of shear stresses parallel to the surface is not affected by the direction of traction, the distribution of such stresses could be obtained by combining shear components associated with both normal and tangential forces. These components for several surface and subsurface planes are shown in Figures 8(a) and (b).

On the surface, where no residual stresses exist, the shear stress is an inverted symmetric cycle whose stress-strain relationship is shown in Figure 9(a). At some depth below the surface the resultant shear stress distribution is obtained as an asymmetric cycle whose stress-strain relationship exhibits plastic strain in both cyclic and monotonic form, as shown in Figure 9(b). Yet, at greater depths the influence of the tangential loading diminishes even further. The resulting shear stress in such a layer corresponds to the normal force in that it is fully reversed, thus insuring that the plastic strain in these regions is almost completely cyclic, see Figure 9(c). Based on this description of the stress-strain cycles in the railhead, confirmed by the work of Hahn and co-workers [Ref. 11], the following mechanisms for fatigue damage can be suggested.

At the depth of less than 100 μm or 1 mm, in the cases of our discs of full size rail, respectively, the deformation is controlled by the ratchetting pattern [Fig. 9a]. It is manifested by the appearance of heavily deformed, displaced layers accumulating along the gauge corner of the outer, and field side of the inner, rail disc, an example of which is shown in Figures 10(a) and (b). The surface cracks could, due to fracture by plastic instability, initiate at the surface defects and propagate inward along shear planes in transgranular pattern, in the presence of a compressive stress field. These cracks, when branching or intersecting, lead to the removal of flakes of rail material, as seen in Figures 10(a) and (b).

In the layer lying below the one discussed above, the thickness of which may vary along the width of the rail disc, a mixed ratchetting-cyclic strain exists in sequential loading cycles as indicated in Figure 9(b). Damage could then be expected to occur by ratchetting and fatigue. This combined damage mode could explain the formation of deeper shelly spots or spalls. In this mode cracks nucleate around voids or inclusions and propagate due to repetitive cyclic strain. The propagation rate is accelerated by the presence of ratchetting. When the crack reaches a certain length it propagates toward the free surface in multiple steps along shear and normal planes. Upon reaching the outer surface layer, sudden fracture takes place due to surface plastic instability, resulting in brittle type failure. This mechanism is illustrated in Figures 11(a) and (b).

At the boundary between the plastically deformed zone and the undeformed metal, about 200 to 500 μm (2 to 5 mm in the case of full-scale rail), the deformation is dominated by reversible cyclic strain. In such layers, voids and inclusion-matrix interfaces could act as the origin of short cracks that, depending on the cyclic plastic strain amplitude, could be arrested (cyclic hardening material) or continue to grow (cyclic softening material). In the latter case, when the propagating crack reaches the outer surface or links with a surface crack, deep shelling could appear.

These mechanisms, with the depth ranges as described above, are valid for the conditions of dry rolling contact. In this case, the outer surface layer may experience resistance to forward deformation (monotonic hardening) leading to deceleration of the damage process. Under lubrication, however, the magnitude of the surface shear stress is reduced, permitting a combination of ratchetting-fatigue to act on the surface layer. As this layer cycle softens, the rate of fatigue damage is increased.

A major element in quantifying these mechanisms is the deformation characteristic of the individual layers under various loading and lubricating conditions. Such a study, which is beyond the scope of this paper, is detailed in Reference 12.

5.0 CONCLUDING REMARKS

An attempt was made, using a laboratory apparatus, to evaluate the response of several steel types to rolling contact conditions under dry and lubricated environments. It was observed that resistance to dry wear generally increases as a function of the hardness; such an observation has been made by other investigators. Wear rate measurements were also in agreement with data obtained from a controlled full-scale system. Furthermore, a statistical approach to calculate crack length density was used to identify the fatigue damage in the matrix of the tested discs. Such an approach, while criticized as a destructive technique, was capable of qualitatively evaluating the fatigue resistance of tested materials. An interesting result, however, was that while lubrication has a positive effect, as expected, in reducing surface wear, it could decrease the resistance of subsurface layers to fatigue damage. A qualitative model based on the description of the stress-strain relationship in surface and subsurface layers of tested discs was then introduced to explain such an observation.

6.0 REFERENCES

1. Roney, M.D. — "Economic aspects of the wear of rail on Canadian railways". Contact Mechanics and Wear of Rail Wheel Systems, J. Kalousek, R.V. Dukkipati and G.M.L. Gladwell, eds., University of Waterloo Press, 1983, 271-292.

2. Beagley, T.M. — "Severe wear of rolling/sliding contacts". Wear Vol. 36 (1976), 317-335.

3. Bolton, P.J. Clayton, P. — "Rolling-sliding wear damage in rail and tyre steels". Wear Vol. 93 (1984), 145-165.

4. Kalousek, J. — "Contact geometry between wheel flange and rail". National Research Council of Canada, Division of Mechanical Engineering Technical Report TR-WE-41, NRC No. 23208, March 1984.

5. Johns, T.G. et al. — "Engineering analysis of stresses in railroad rails". Batelle Columbus Labs., Report FRA/ORD-81/51, Oct. 1981.

6. Ghonem, H. Gonsalves, R. — "Comparative performance of type II trucks". Department of Research, Canadian Pacific Ltd., Report No. S576-78, Nov. 1978.

7. Kalousek, J. Rosval, G. Ghonem, H. — "Lateral creepage and its effect on wear in rail wheel interface". Contact Mechanics and Wear of Rail/Wheel Systems, J. Kalousek, R.V. Dukkipati and G.M.L. Gladwell eds., University of Waterloo Press, 1982, 373-393.

8. Steele, R.K.
Reiff, R.P.
"Rail: its behaviour and relationship to total system wear".
Proceedings of the FAST Engineering Conference, 1981, Report No. FRA/TTC 82/01, 115-174.

9. Ghonem, H.
Kamaph, S.
"Effect of mean stress on the fatigue crack initiation life of .8% carbon steel".
Presented at ASME-PVP Conference, San Antonio, Texas, June 1983.

10. Smith, J.O.
Liu, Ch.K.
"Stresses due to tangential and normal loads on an elastic solid with application to some contact stress problems".
Journal of Applied Mechanics, Transactions of the ASME, 75, June 1953, 157-166.

11. Hahn, G.T.
Bhargava, V.
Yoshimura, H.
Rubin, C.
"Analysis of rolling contact fatigue and fracture".
Submitted to the Sixth International Conference on Fracture, Dec. 1984.

12. Ghonem, H.
Steele, R.K.
"Study of Ratchetting-low cycle fatigue in AISI 1080 pearlitic steel".
Submitted to International Journal of Fatigue.

(a)

(b)

Fig. 1: (a) Dry gauge face wear on outer rail (side cutting)
(b) Flaking and spalling on the inner rail

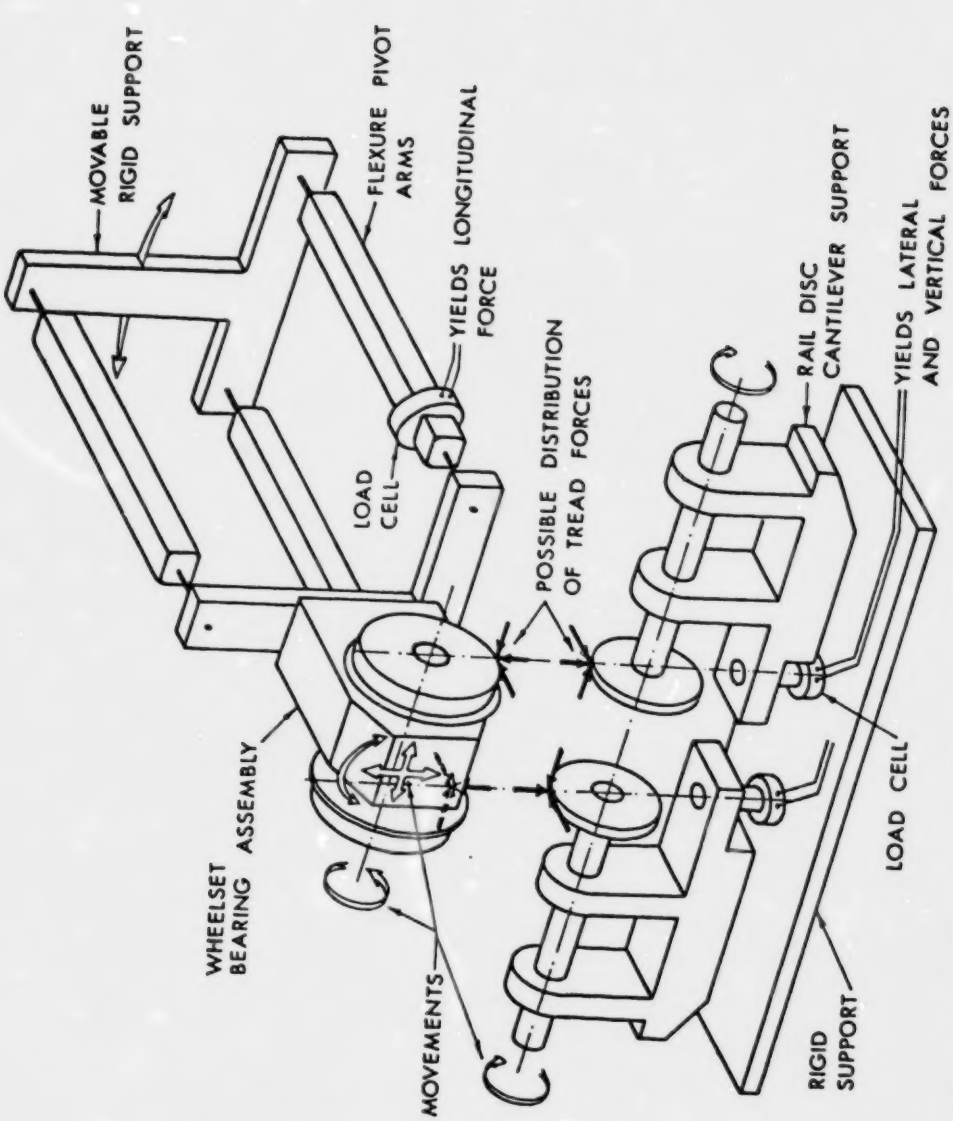

FIG. 2: SCHEMATICS OF RAIL WHEEL WEAR TEST APPARATUS

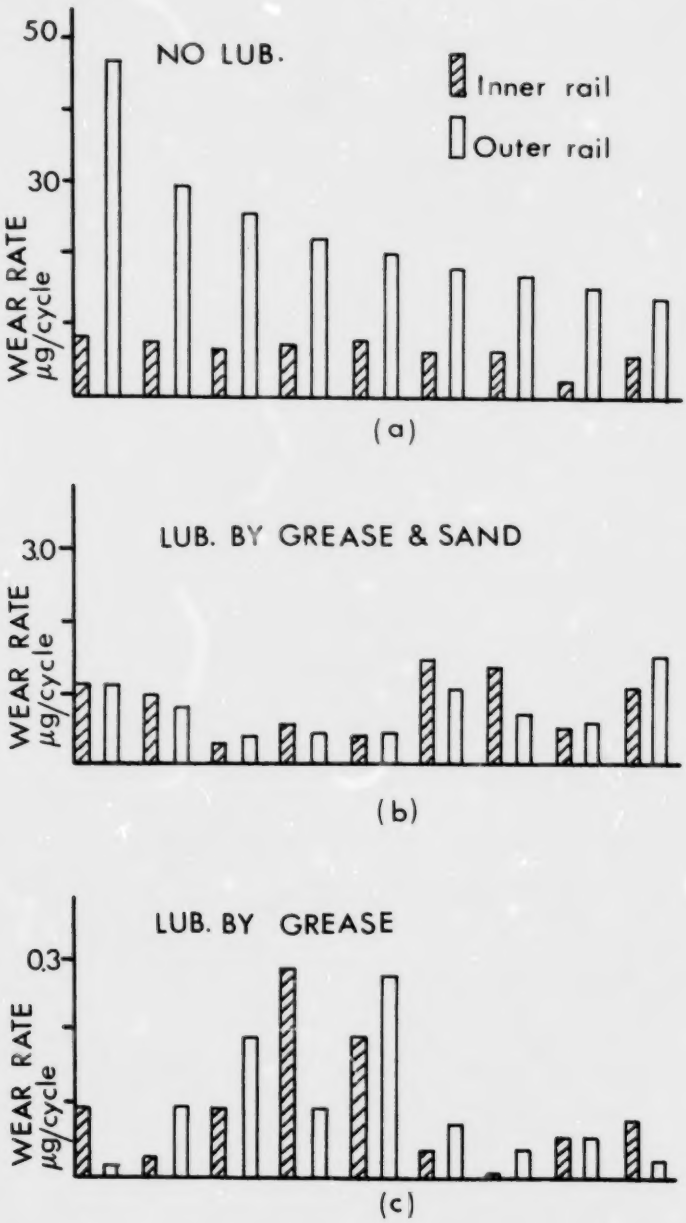

Fig. 3 Rate of material removal at
(a): no lubrication
(b): grease sand and
(c): grease only lubrication

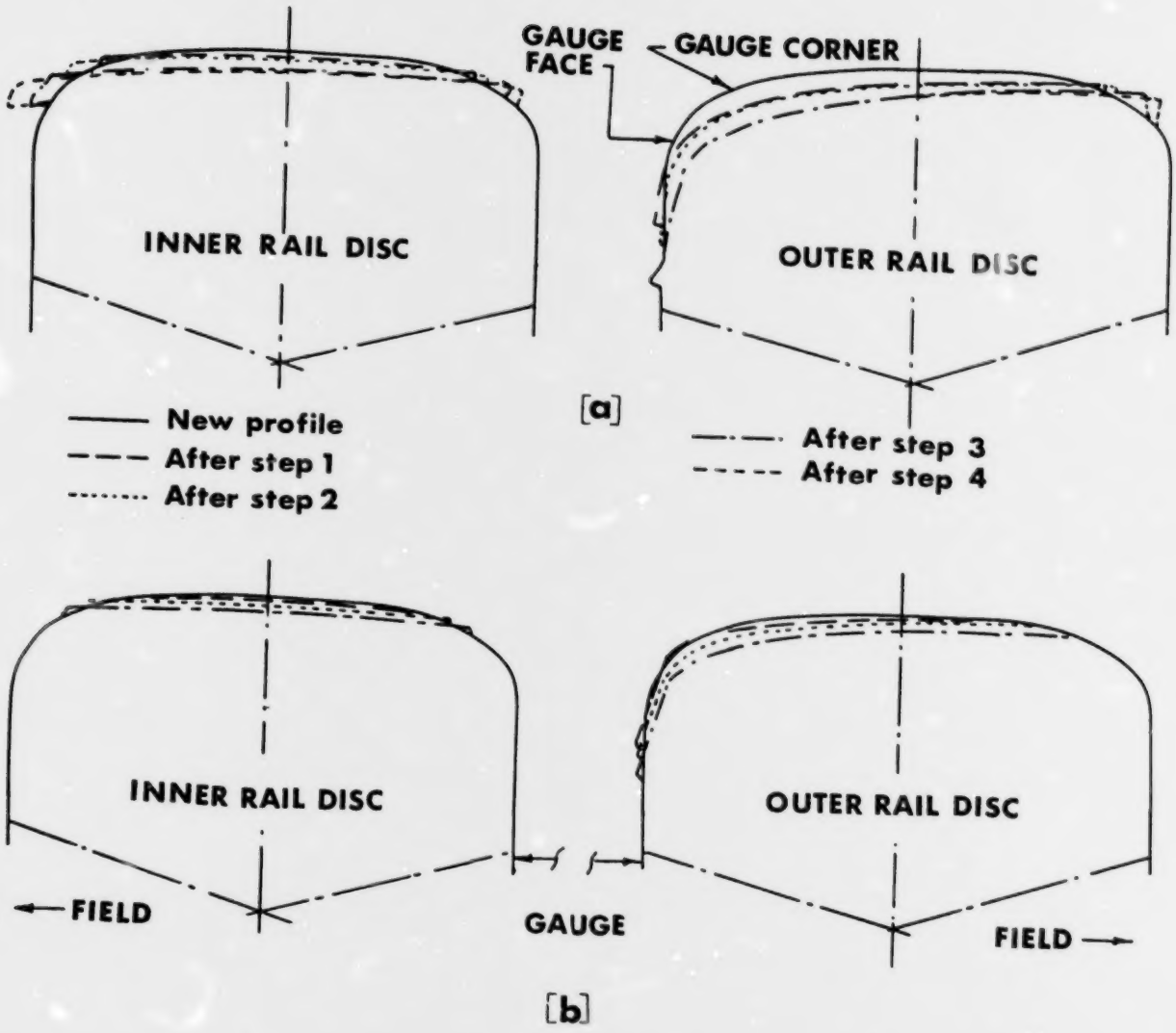

Fig. 4: New and worn profiles of inner and outer rail discs (a): Specimens A (b): Specimens I

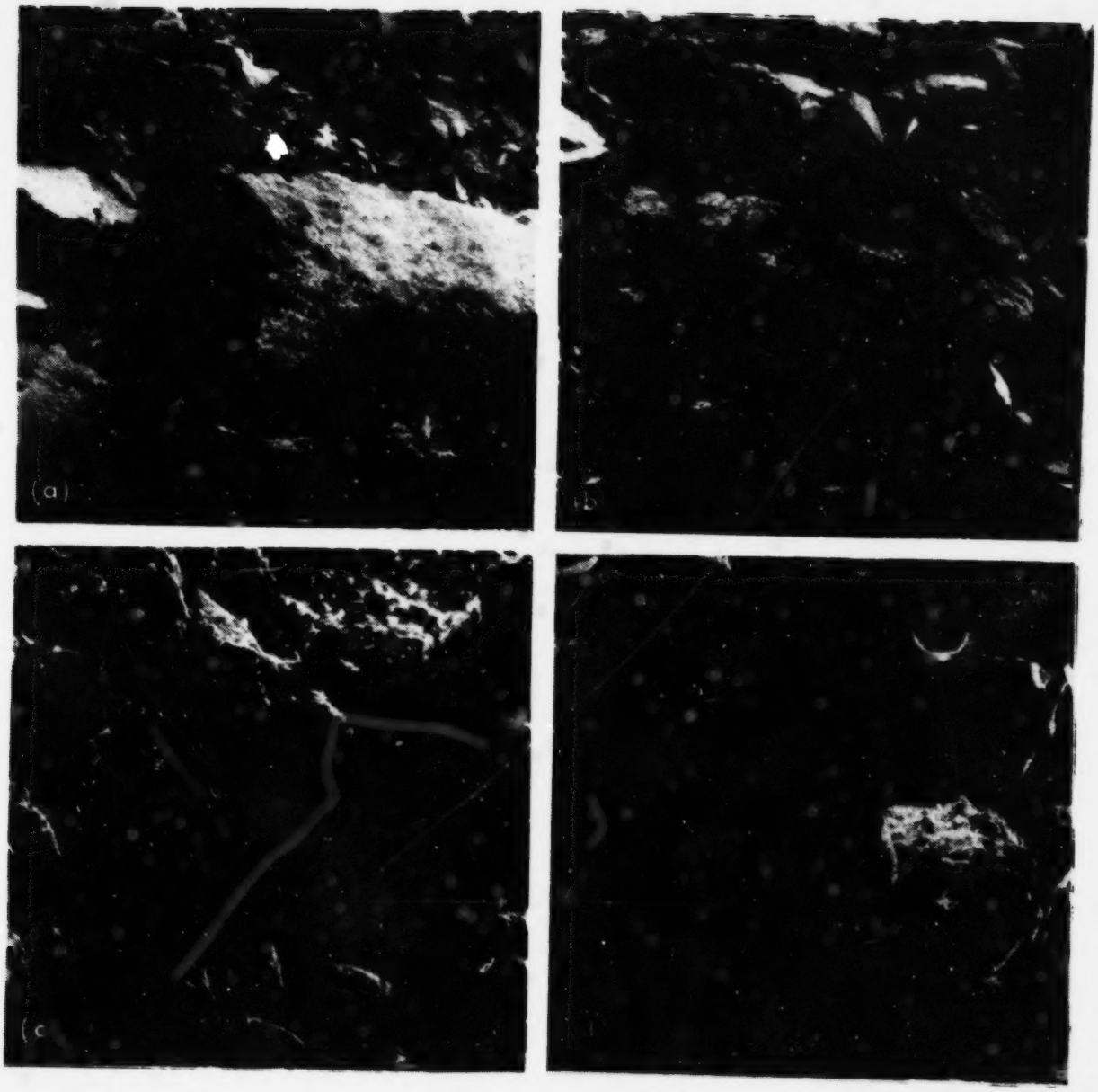

Fig. 5: Wear debris (a) no lubrication - outer rail disc A
(b) no lubrication - outer rail disc I
(c) grease-sand lubrication - outer rail disc I
(d) grease only lubrication - outer rail disc A

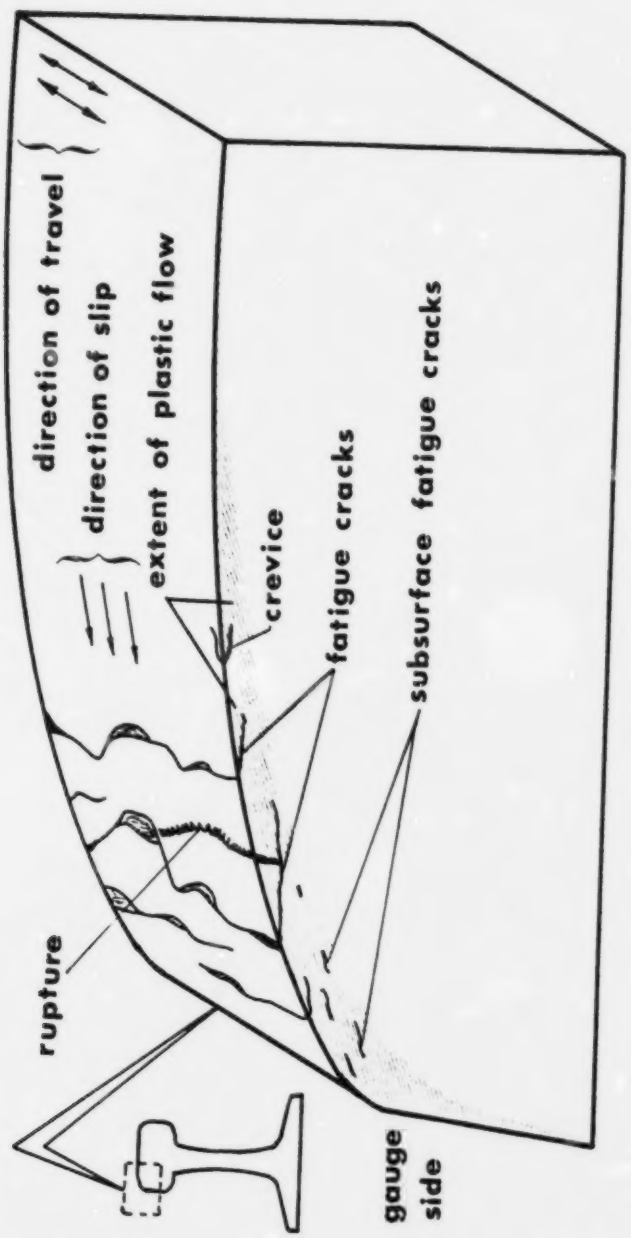

Fig. 6: Schematics of contact fatigue damage on the outer rail or rail disc

Fig. 7: Cross section at a gauge corner of outer rail disc Specimen G

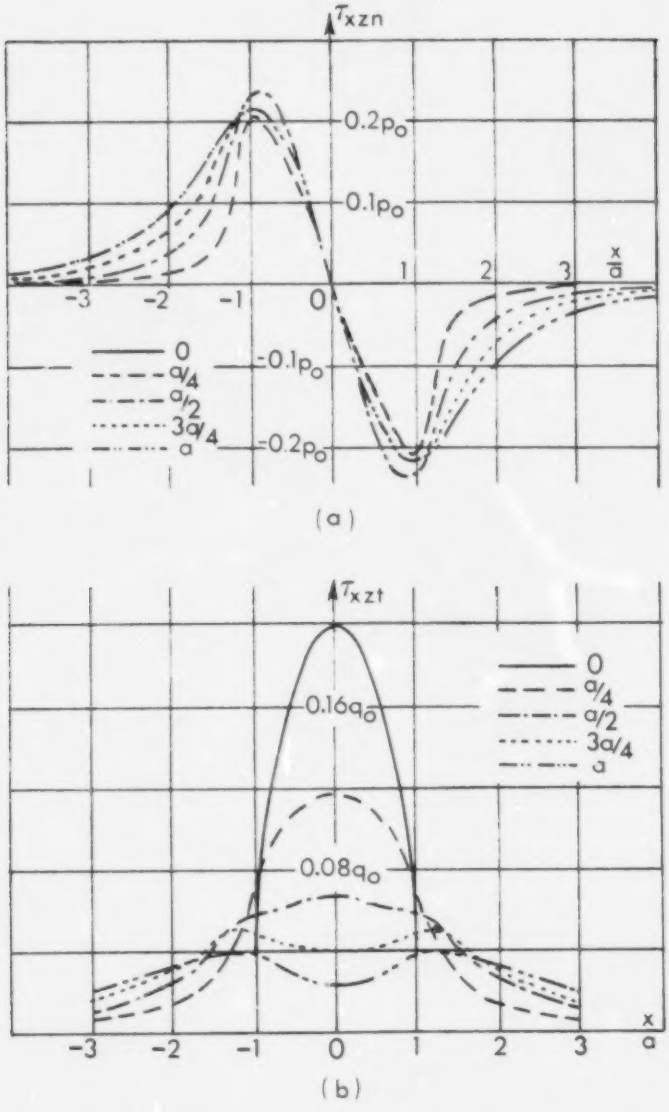

Fig. 8 Stresses due to (a): normal and (b): tangential loads (After Smith and Liu (10)).

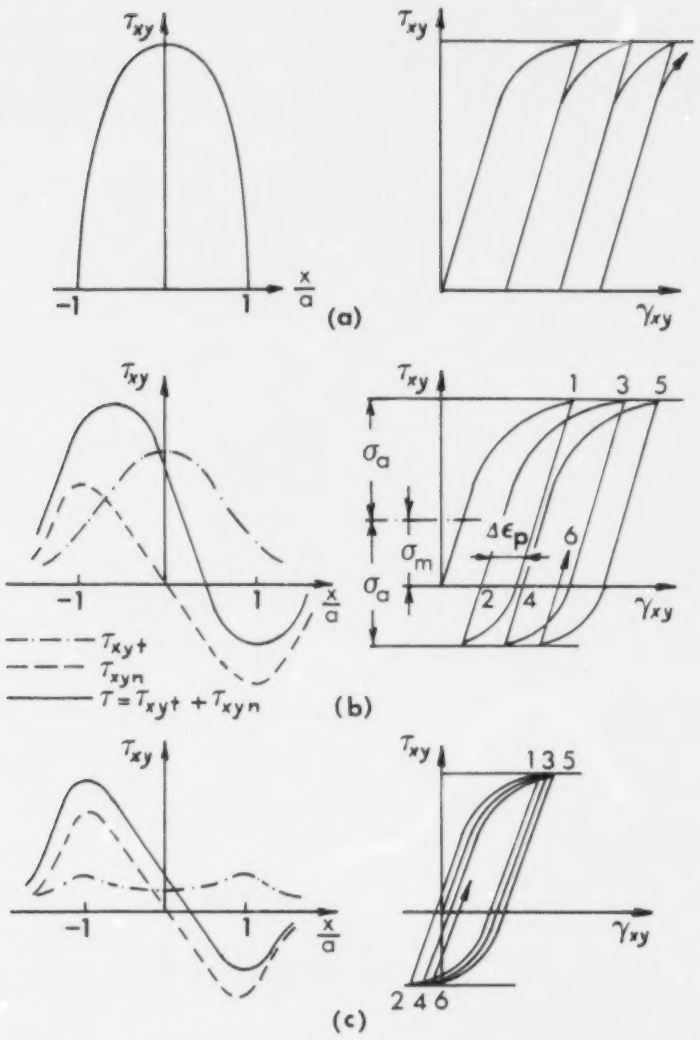

Fig. 9: Shear stress distribution and associated stress-strain cycle at
(a): immediate surface layer
(b): subsurface layer and
(c): deep subsurface layer

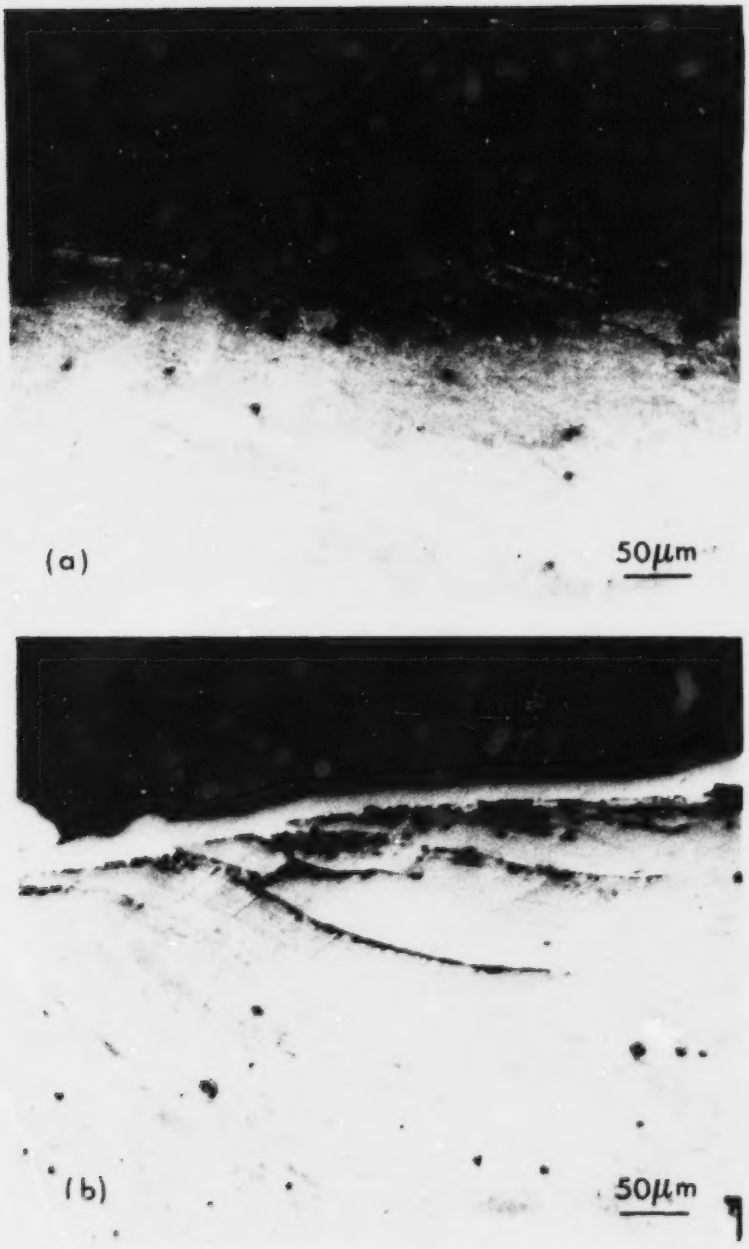

Fig. 10 Contact fatigue damage of
(a): top surface of inner rail disc A
(b): gauge corner of outer rail disc E

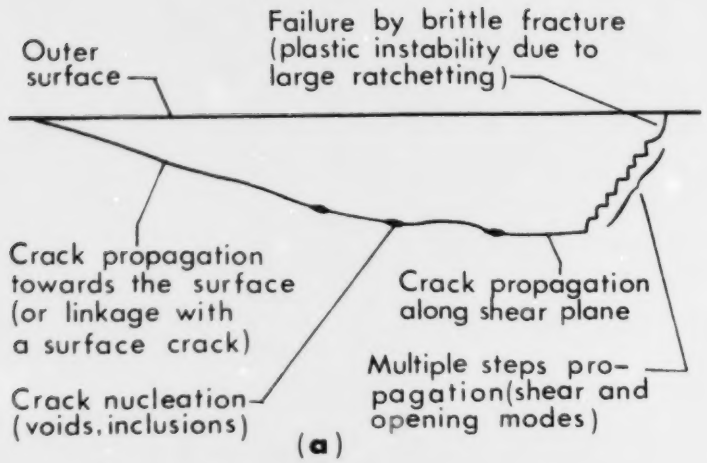

Fig. 11 (a): Schematics of flake initiation, growth and release mechanism
(b): An example of flake before its release at the gauge corner of outer rail disc I

PART II

THE WEAR RESISTANCE AND WORN METALLOGRAPHY OF PEARLITE, BAINITE AND TEMPERED MARTENSITE RAIL STEEL MICROSTRUCTURES OF HIGH HARDNESS

THE WEAR RESISTANCE AND WORN METALLOGRAPHY OF PEARLITE, BAINITE AND TEMPERED MARTENSITE RAIL STEEL MICROSTRUCTURES OF HIGH HARDNESS

1.0 INTRODUCTION

It is generally believed that increasing rail hardness and strength increases rail wear resistance. This belief is substantiated by test data from North American and Australian railways [Refs. 1-4] and is reflected in the many studies done to develop high strength steels for premium rail by accelerated cooling [Refs. 5-7] and alloying [Refs. 8-10] of basically standard C-Mn eutectoid compositions. The most frequent cause of high (or outer) rail replacement on curves is gauge-face wear and this increases with increasing axle load and lateral creepage (decreasing curve radius). Thus, Roney's [Ref. 11] 1982 review on the economic aspects of wear on Canadian Railways states that:

1. The great majority of the replacement rails scheduled for 1982 will be laid in the heavy tonnage, high curvature regions of main line track, and

2. A significant percentage of the replacement rails will have superior strength and hardness compared to the replaced rails.

Current premium rails range in hardness from ≈ HRC 36-39 (HV 354-382). It is thought by some rail manufacturers and users that increasing the hardness to HRC 43-45 (HV 423-446) may further significantly reduce wear rates and be economically viable. However, preliminary, full-scale results [Ref. 12] obtained under controlled conditions at the Facility for Accelerated Service Testing (FAST), Pueblo, Colorado, suggest that wear resistance only increases slowly with increasing hardness from HRC 37 (HV 363) to HRC 39.5 (HV 387). Somewhat similar results were obtained by Hodgson et al [Ref. 13] for the abrasive wear rate vs. original hardness. It was, therefore, considered desirable to investigate the effects of three hardness levels, HRC 38, 42, 45 (HV 372, 412, 446) representing the possible hardness range of the next generation of premium rails, on the wear rate of one particular steel to determine whether the production of very hard rails is actually economically justifiable. Furthermore, although studies [Refs. 14-16] of the effect of microstructure on wear resistance indicate that fine pearlite is superior to bainite or tempered martensite, the hardnesses examined were lower than those proposed in the present work. Hence, the scope of the experiments undertaken was expanded to include the testing of bainite and tempered martensite as well as pearlite.

2.0 EXPERIMENTAL PROCEDURE

2.1 Test Rig

Wear and contact fatigue tests were carried out on a disk-on-disk rail/wheel wear apparatus designed to simulate the interaction between a railway wheelset and a pair of rails. The rails were modelled by disks, 69.9 mm in diameter, fabricated from the heads

of full size rail. The crown of each disk was machined to a new 67.5 kg. m^{-1} (136 lb. $yd.^{-1}$) AREA profile using a numerically controlled lathe. The wheelset was modelled by disks 120.7 mm in diameter at the centre of the tread, machined to a worn wheel profile designated "CN Profile A", and rigidly mounted on a shaft. Both rail and wheel profiles were reduced ten times in cross section. The test rig has been described in detail by Kalousek [Refs. 18 and 23].

The orthogonal components of the load vector transmitted to the rail disks were measured by load cells. The distribution of forces between flange and tread contacts, occurring between disks representing the high (outer) wheel and rail in a curve was determined by computation [Ref. 17]. The wheelset loading was selected to yield Hertzian contact stresses of a magnitude representative of field conditions. The maximum Hertzian pressure, p_o, between worn rail statically loaded by a laden car with worn wheels on a tangent track, is approximately 830 MPa. However, the contact stresses which occur in curves are much higher. Considering the contact between the wheel's flange root and the gauge side of the high rail or between the wheel's false flange and the field side of the low rail, the calculated range for p_o is between 1,500 and 3,000 MPa. To simulate these high values of p_o, the wheelset load during all tests was 7,000 N (1,570 lbf) yielding p_o = 1,800 MPa (261 ksi) for the case of two symmetrically loaded contact areas. This load and the resulting p_o produced a work hardened layer in the rail disk equivalent to that observed in a full-scale rail.

2.2 Materials

All wear blanks were machined from the railhead of an experimental Cr-Mo rail, austenitized at 1,025°C and isothermally transformed in a salt bath. The steel was of composition, 0.72% C, 0.81% Mn, 0.28% Si, 0.022% S, 0.79% Cr, 0.21% Mo and transformation temperatures were 625°C (HRC 38), 595°C (HRC 42) and 575°C (HRC 45) for pearlite, and 460°C (HRC 38), 415°C (HRC 42) and 375°C (HRC 45) for bainite. Transformation details are given by Fegredo et al [Ref. 19] and the isothermal transformation temperature diagram of this steel is also given by Stone [Ref. 1]. However, because of random Mo segregation and the corresponding localized increase in hardenability, some martensite streaks appeared in the upper bainite disks of hardness, HRC 38 (HV 372). This occurred even though longer transformation times were generally imposed than those determined by the isothermal transformation experiments [Refs. 1 and 19]. Tempered martensite microstructures were obtained by austenitizing at 1,025°C, oil-quenching and then tempering the blanks for one hour at 510°C (HRC 45), 566°C (HRC 42) and 616°C (HRC 38).

All wheel disks were made from AAR Class C wheel steel, having the same chemical composition as plain carbon rail (similar to 1070 steel) and hardness HRC 38 (HV 372).

2.3 Wear Tests

"Full sequence" tests consisted of sixty periods of 40,000 revolutions of the rail disks. Within each period, the yaw misalignment was altered to apply angles of attack of 10', 18', 32' and 40'

successively, for 2,500 revolutions each. These angles represent the mean yaw misalignment measured on the trailing and leading axles, of trailing and leading freight car trucks, respectively, in a curve of 235 m radius (8° curve) [Ref. 20]. The angles-of-attack were next decreased successively, to complete a total of 20,000 revolutions. The machine was then stopped, the direction of disk rotation reversed and the yaw angles changed from positive to negative values to maintain the same orientation of curvature. A second sequence of 20,000 revolutions was run in this manner to complete a period of 40,000 revolutions. Each period was roughly equivalent to 10^6 gross tons (1 MGT) of service for rails laid in a 235 m radius curve in single main line track and experiencing heavy axle load traffic in both directions. The sixty periods were applied as follows:

1. One period run dry at an ambient temperature of 18°C and 45% relative humidity. The disk surfaces were contaminated by oxidized wear debris generated during the course of this period. Rail disk speed, 250 rpm.

2. Nineteen periods, lubricated by a calcium soap base grease containing mineral oil, having a viscosity at atmospheric pressure of 0.02 Nsm^{-2}, 11% graphite and 2.5% MoS_2, added by the manufacturer as an EP additive. In addition, 20% of the sand was added to the grease during the test to simulate the dispensation of sand by locomotives. The limiting coefficient of friction for this type of boundary lubrication was typically 0.18. Rail disk speed, 500 rpm.

3. Disks were cleaned and Step 1 repeated.

4. The final 39 periods were run as in Step 2, but with pure grease (no sand). It was found by experience that a small quantity of grease, when transferred from a reservoir to each rail/wheel pair every 4,000 revolutions, remained from application to application. The grease was, however, contaminated by wear particles, yielding a boundary lubrication regime with a limiting coefficient of friction in the range, 0.09 - 0.12. This grease-only lubrication regime, although less typical of field conditions than the grease/sand lubrication, was used to enhance the rate of contact fatigue damage to the rail disk.

Wear was measured by removing both rail disks periodically and weighing them. At the same time, disk profiles were obtained with a precision of ± 2 μm using an electronic profilometer. The superposition of profiles taken before, during and after the test helped to identify the locations from which metal was removed and the locations to which metal was displaced due to plastic flow.

In addition to full sequence tests, as described, one pair of pearlite disks and one pair of tempered martensite disks were subjected to two periods of dry wear only. Table 1 (page 2-16) summarized the materials and the test sequences used.

2.4 Metallography

Transverse sections were cut from the worn disks, nickel plated for edge retention, and polished and etched using standard techniques for both optical and SEM observations. Microhardness measurements were made with a diamond pyramid indenter at a load of 100 grams (0.98 N).

An image analyser (Cambridge Instruments Quantimet 900) was employed to measure the number and length of "cracks" within 150 μm depth from the Ni-steel interface on transverse sections from four high-rail disks. The features counted by the Quantimet were surface cracks and cracks at deformed inclusions, principally MnS, within the disk. Features less than 10 μm were not counted and a horizontal amender was used so that features within 10 μm of each other in the same length direction were joined and considered as one feature. However, only a few were joined.

To obtain thin foils for TEM at the worn surfaces and and at known distances below the surface, transverse samples were again cut from the worn disks, and electroplated with nickel for edge preservation.

Disks were cut from the plated samples, mechanically thinned and finally jet-polished, to obtain a perforation and thin area as close as possible to the sample/Ni interface.

3.0 OBSERVATIONS

3.1 Wear Tests

3.1.1 Wear rates

Wear rates of the different microstructures and hardnesses are given in Figure 1 for the three environments employed. The following points are apparent:

1. The wear rate of the high rail disk decreases with increasing hardness in dry wear for tempered martensite and bainite structures, but not significantly for pearlite.

2. The high rail disk microstructures can be rated in the following order of decreasing dry wear resistance: pearlite, bainite, tempered martensite. In particular, tempered martensite of hardness HRC 38 wears roughly ten times faster in dry wear than pearlite of HRC 38.

3. All low rail disks have similar dry wear rates which are significantly lower than those for high rail disks. Thus, microstructure and hardness appear to have little effect on low rail dry wear rates.

4. Wear rates are markedly lower in a grease - 20% sand environment than in dry wear for both high and low rail disks (note the different wear rate scales on Figures 1a, b and c)

with low rail disks wearing somewhat faster than corresponding high rail disks. Microstructure and hardness do not appear to have a significant effect on the wear rate. (Note: it should be mentioned that the disks representing wheels had to be changed after the first dry wear test (1st period) for the upper bainite disks "D" of hardness HRC 38. This may account for the relatively high wear rate shown in Figure 1(a).

5. Wear rates in a pure grease (fully lubricated) environment are considerably lower than in grease-sand. Again, microstructure and hardness do not play significant roles in deciding wear performance, but high rail disks consistently wear faster than corresponding low rail disks. The wear rate of the tempered martensite high rail disk, A-HR, is almost three orders of magnitude lower in the fully lubricated, than in the dry wear environment.

3.1.2 Wear profiles

The wear profiles determined after each of the four wear stages are shown in Figure 2 for the high and low rail disks of the three microstructures of hardness, HRC 38, (A,D,G). Very little change is visible between the end of the second "no lub. run" (Step 3) and the end of the "grease only" run (Step 4), consistent with the very low wear rates shown in Figure 1(c). All low rail disks appear to behave similarly, but a marked difference occurs between the pearlite (G-HR), and the bainite and tempered martensite (D-HR and A-HR) high rail disk profile changes. The latter develop pronounced shoulders through wear attrition at the lower end of the gauge face, while the pearlite disk develops a shear lip which forms by metal flow. The large profile change for disk D-HR, in grease-sand, is connected with the relatively high wear rate mentioned above. Comparable profile changes are seen in the region between the centre of the running surface and the field corner.

Profile changes for disks of higher hardness were similar to those seen for the tempered martensite and pearlite disks of hardness HRC 38. Thus, shoulders and shear lips developed in the tempered martensite (B-HR and C-HR) and pearlite (H-HR and I-HR) disks respectively, although the extent of the profile changes reflected the respective wear rates. However, the bainitic disks, E-HR and F-HR, developed shear lips on the gauge face instead of on the shoulders, possibly reflecting their improved dry wear resistances.

3.2 Metallography

3.2.1 Optical and SEM

A survey of transverse sections shows that a severely deformed sheared layer exists at the wear surface of all disks. The deformation pattern indicates that high lateral creep forces are imposed, as expected, which produce a pattern of deformation very similar to that observed in full-scale rails on curves [Ref. 21]. The approximate depths of gross shear deformation, at different locations, are given in

Table 2 for all high rail disks, and these increase from 0 μm at the field corner to several hundred μm at and near the gauge corner. The values obtained for J-HR (dry wear) are similar to those of G-HR (full sequence) but much higher values are obtained for K-HR (dry wear) than for A-HR (full sequence). Note that these values are somewhat subjective, and vary with the precise location chosen around the worn surface periphery. Similarly, microhardness values obtained on worn disks depend on the precise location of the traverse, [Figs. 9 and 10]. Relatively shallow shear layers were observed on low rail disks. They were deepest at the centre of the running surface and similar to those observed for the center of the running surface of high rail disks, see Table 2.

The SEM micrographs presented herein concentrate on typical pearlite and tempered martensite microstructures which gave the extreme wear rates.

Figure 3 shows the gauge corner deformation observed in disks, K-HR and J-HR. Note the shoulder which has developed on disk K-HR, compared to the shear lip on disk J-HR (arrows). The depth of gross deformation is more easily seen in the pearlite sample, J-HR.

Figures 4(a) and (d) show gauge corner deformation typical of all high rails tested. The numerous cracks which are apparent in these micrographs were usually associated with MnS inclusions. Both the numbers and lengths of the cracks observed varied systematically with the microstructure and with the test conditions, although all samples were fabricated from the same steel, and should thus have the same number of MnS inclusions. Figure 5 shows image analyser data giving feature (crack) frequency vs. length of feature. These data were obtained from fields covering the gauge face, gauge corner and about a quarter of the width of the running surface, where most wear takes place. The measurements confirm what is seen qualitatively in the micrographs, that more and longer cracks are generated in dry wear in tempered martensite than in pearlite, and that subsequent lubricated service (e.g. the full sequence tests) results in fewer cracks. Presumably, some of the cracked surface layers are worn off, and then fewer cracks are generated due to the lower lateral creepage forces in lubricated operation.

Figure 6 shows the association of cracks with inclusions in more detail. Figure 6(c) shows that undeformed oxide inclusions (Al, Si, Ca, Mn oxide) were also associated with microcracks, although these were much less frequently observed.

At higher magnifications, the effect of deformation on the microstructure and especially on the carbide morphology and spacing, becomes more apparent. Figure 7 shows the original microstructures and Figure 8 shows the near surface microstructures which developed. The very fine carbide spacing in the pearlite samples, J-HR and G-HR, compared to the tempered martensite samples, is remarkable. The microstructure developed in the bainite disk, D-HR, is intermediate between the pearlite and tempered martensite full sequence disks. A bainitic microstructure was not subjected to a dry-wear-only test.

Low rail disks showed much shallower regions of gross deformation, and fewer cracks.

3.2.2 Microhardness measurements

All high rail and low rail disks tested were subjected to microhardness tests, and the results shown in Figure 9 are typical. As mentioned above, the microhardness values obtained are quite sensitive to the location of the microhardness traverse. A second set of microhardness values was taken at the gauge corners of samples, K-HR and J-HR, to correlate with TEM observations (see below). These data are shown in Figure 10 (page 2-32) where it can be seen that higher hardnesses are observed near the surface of disk J-HR than those shown in Figure 9b. The values obtained for disk K-HR in Figures 9(b) and (10) are comparable. In general, the following points are observed:

1. The specimens are hardest at, and very close to, the worn surface. Hardness decreases with increasing depth and generally approaches the hardness of the undeformed microstructure at between 50 and 250 μm.

2. The highest values are obtained at the gauge corner.

3. The specimens subjected to dry wear only, i.e., J-HR and K-HR, have the highest hardness and the pearlitic specimen, J-HR, is consistently harder than the tempered martensite specimen, K-HR, at, and near, the worn surface. In particular, extremely high values of HV_{100} 750-919 (HRC 62-67) are obtained for J-HR at the worn surface in the centre of the gauge corner, and this level of hardness persists for at least 50 μm.

4. The bainite disk, D-HR, consistently hardnes less than the tempered martensite (A-HR) and pearlite (G-HR) disks for full sequence test specimens.

The hardening pattern for high rail disks of undeformed hardness, HRC 45, generally parallels that in Figure 9. Their hardness values appear to reflect their higher intrinsic hardness. With regard to low rail disks, Table 3 shows that the hardest values of the low rail disks are produced at the worn surface for the dry wear specimens, J-LR and K-LR, but these disks have similar hardness values to the others beneath the surface. Comparisons between disks of similar microstructure, but different undeformed hardness, i.e., A-LR and C-LR, D-LR and F-LR, G-LR and I-LR, show that they undergo more or less the same degree of work hardening.

3.2.3 TEM

Thin foils for transmission electron microscopy were prepared from all disks subjected to the full sequence wear test, and, in addition, two stage carbon replicas were prepared from polished and etched sections of samples, J-HR and K-HR. A much lighter etch was used for the samples to be replicated than for the samples examined in the SEM (above). The principal results are:

1. There is significant deformation of the cementite in the bainitic and pearlitic disks, near the surface, but little, if any, deformation of the cementite in the tempered martensite disks.

2. In agreement with SEM results, significant refinement of the carbide spacing is observed near the worn surface, especially for the pearlite as shown in Figure 8.

3. There is a very great refinement of ferrite grain size near the worn surface.

4. A texture is observed in the near surface region of all specimens. This is manifested by a weak or absent {200} ferrite diffraction ring, suggeting a <111> wire texture.

Figure 11 shows a region of disk, H-HR, 30 μm below the running surface. Very fine, unbroken cementite lamellae are seen, with individual spacings as small as 20 nm, demonstrating that there has been deformation of the cementite. The rings on the diffraction pattern, from a region 3.5 μm in diameter, show that the grain size is much finer than 3.5 μm, and the weak {200} ring suggests texture.

Figure 12 shows a thin foil from disk E-HR, between the gauge corner and the centre of the running surface. The interface between the sample surface and the Ni electrodeposit is clear. The dark field micrograph, [Fig. 12b], shows the extremely fine grains which have developed, as does the smoothness of the diffraction rings in Figure 12c, where an aperture defining a selected area of only 0.9 μm was used. Again, there is the suggestion of texture, both in the weakness of the {200} ring, and in the presence of thickened regions on the {110} and {211} rings.

Figure 13 shows a region of disk A-HR, 70 μm below the running surface. A definite cell or fine grain structure has again developed in the ferrite, but no so fine as seen in the pearlitic (H-HR) or bainitic (E-HR) samples. Also, there is little suggestion of deformation of the cementite.

Figure 14 shows the refinement of the carbide spacing near the surface, as well as some breakup of cementite lamellae in the pearlite sample, near the surface. Very little deformation of the carbides in the tempered martensite is seen. Interparticle spacings were measured on numerous such micrographs, and the results are plotted in Figure 15. For interlamellar spacings in the pearlite, a simple linear intercept was used, since the structure was well aligned near the surfce. At greater depths, below the region of gross deformation referred to above, the test line was maintained normal to the lamellae as seen on the replica, and the narrowest spacings only were measured to ensure that only lamellae nearly perpendicular to the replicas were considered. This procedure was adopted, since, at the high magnification required to clearly resolve the lamellae, insufficient colonies were seen in any one field to permit the use of statistical techniques such as suggested by Underwood. For the tempered martensite carbide spacings, the formula:

$$\lambda = \frac{(1 - V_v)}{N_L} \qquad (1)$$

given by Underwood [Ref. 22] was used. Here,

λ is interparticle distance

V_v is volume fraction of particles (obtained from point counts on the replicas)

N_L is the number of interceptions of particles, per unit length of test line

Comparing Figures 10 and 15, it is apparent that the very high hardness of pearlite is associated with very small interlamellar spacing. The hardness of tempered martensite stems from the deformed substructure with a contribution from particle-(carbide) hardening so that finer carbide spacings can also be associated with higher hardness.

4.0 DISCUSSION

Full-scale rail wear tests are enormously expensive and time consuming. Thus, a laboratory-scale test which correlates well with field data is of particular interest. The tests used in the present work are similar to those done by Kalousek et al. [Ref. 23] on specimens machined from seven different commercially available standard and premium rails. The rails had also been subjected to full-scale tests [Refs. 12 and 24] on the FAST track Using the Figure of Merit (FM), criterion proposed by Steele and Reiff [Ref. 24] as a measure of gauge face wear resistance, very similar FM ratios were obtained in both laboratory and full-scale tests of head hardened, fully heat treated and standard rail steels indicating a good correlation between laboratory and field results.

In the present work, tempered martensite, bainite and pearlite have been examined in the hardness range, HRC 38-45. Both tempered martensite and bainite show improved dry wear resistance with increasing hardness, but the dry wear resistance of pearlite is essentially independent of hardness. Furthermore, pearlite has the highest wear resistance [Fig. 1a]. Since increasing hardness decreases fracture toughness these results satisfy both experimental objectives, i.e., to determine the best microstructure and the maximum useful hardness. We conclude that: (a) fine pearlite should continue to be used in premium rails in preference to tempered martensite or bainite, and (b) no useful purpose is served in achieving a hardness beyond HRC 38-40.

The reduction of friction coefficients to 0.18 and 0.09-0.12 by grease-sand and pure grease lubrication, respectively, markedly decreases wear rates in all microstructures. The pure grease run follows one period (40k revs) of dry wear in the full sequence tests. This means that stress systems in the lubricated environment are imposed on a cracked surface characteristic of dry wear.

The maximum shear stress occurs at or below the surface, depending on whether the friction coefficient is greater or less than 0.32 [Ref. 25]. Beagley [Ref. 26] has pointed out that fatigue cracking and rail shelling result when the maximum shear stress occurs below the surface and the loads are sufficiently high. The examination of wear debris released during the pure grease run in similar full sequence tests on pearlitic steels by Kalousek et al. [Ref. 23] has shown that most of the flakes were over 1,000 times the weight loss cycle. Thus, slow subsurface fatigue crack propagation and crack amalgamation of the precracked (by dry wear) specimens must occur over many revolutions before large flakes drop off.

Low rails have significantly smaller wear rates than corresponding high rails under dry wear or pure grease regimes. The hardness/dry wear rate relations of the three microstructures somewhat parallel those of the high rails. The analysis of wheel/rail contact conditions is outside the scope of this paper, however, Kalousek et al. [Ref. 23] concluded from an examination of wear profiles and wear debris that the difference in dry wear rates between low and high rails can be attributed to the difference in wear in the vicinity of the gauge corner. Because the gauge face wear does not occur in low rails [Fig. 2] and the depth of the grossly deformed shear layer at the centre of the running surface is fairly similar to that in high rails, Table 2, wear rates observed in low rails are much less than those observed in high rails.

High work hardening occurs at and near the surface of the worn high rail disks, as shown in Figures 9 and 10, and in Table 3. The greatest hardness values are found in dry wear and at the gauge corner, where the greatest amount of gross deformation is observed. Many surface and subsurface cracks are seen within the deformed subsurface layer, especially in the vicinity of the gauge corner [Fig. 4], so that measured hardness values may, in fact, be conservative if cracks are near the indenter.

The deformability of MnS is well known, together with its adverse effect on toughness, and Bolton and Clayton [Ref. 27] have recently postulated that flaking in their Type 1 dry wear mode is due to deformed MnS inclusions. Using x-ray emission spectroscopy (XES), we have observed that MnS is associated with many or most of the thin subsurface cracks, suggesting that these cracks mainly initiate at deformed MnS within the grossly deformed shear layer. The MnS inclusion/steel interface is very weak so that the inclusion periphery is basically a crack whose aspect ratio increases with increasing deformation on repeated cycling, and as the inclusion moves nearer to the surface. Interfacial cracks are also seen at comparatively undeformed oxide inclusions [Fig. 6c]; these are less common.

Now consider the disks of hardness, HRC 38, for which the greatest differences were found in the dry wear rate. Quantimet measurements, which were made to a depth of 150 μm, show that the total crack length in dry wear is much greater in tempered martensite than in pearlite [Fig. 5].

Further, comparing data from Table 2 and from Figures 1, 9 and 10, we see that for dry wear (or also for the full sequence tests), we may associate, on the one hand, good dry wear performance with a high degree of work hardening, a shallow depth of gross deformation and low total crack length. On the other hand, we correlate inferior dry wear performance with lesser work hardening, greater depth of gross deformation and longer total crack length. Thus, we conclude that it is not so much the initial hardness, but rather the degree of work hardening exhibited by the rail, which controls its dry wear performance.

The reason for the higher degree of work hardening exhibited by the pearlite would appear to lie in the different morphology of the carbides in the two microstructures. Although the pearlite microstructural character changes below transformation temperatures of ≈ 600°C, i.e., the cementite lamellae become increasingly irregular [Ref. 9], their lamellar nature is still apparent for the lowest (pearlitic) transformation temperature of 575°C. They have a high aspect or large surface to volume ratio. Thus, shears in the ferrite are effectively transferred to the cementite, which deforms with the ferrite to produce a very fine lamellar structure, as shown in Figures 11 and 14. Langford [Ref. 28] has studied the refinement of pearlite in wire drawing, and the correlation between pearlite spacing and strength. He concluded that:

$$\sigma = \sigma_o + 0.35\,\bar{G}\left[\frac{b_{cm}}{d}\right]^{1/2} + \alpha\,\bar{G}\left[\frac{b}{d}\right] \qquad (2)$$

where σ_o is the lattice friction stress of ferrite (≈ 175 Mpa), G is the geometric mean of the shear moduli of ferrite and cementite, 7.7×10^4 MPa, b_{cm} is the Burgers vector in cementite, 0.225 nm, b is the Burgers vector in ferrite, 0.248 nm, α is a constant approximately equal to 0.7, and d is the pearlite spacing. If d is set equal to 30 - 35 nm, corresponding to the finer spacings observed in [Fig. 13], then Langford's equation allows us to estimate a maximum microhardness of HV 900 - 1,000, as observed in Figure 10.

In the tempered martensite, on the other hand, the cementite occurs as spheroidal particles, with relatively small surface areas. Thus, shear stresses in the ferrite are not transferred effectively to the cementite, which does not then deform. Although a refinement of the microstructure occurs, including a refinement of the grain size, the carbides are unable to reinforce the ferrite matrix as they do in pearlite, so that the same degree of work hardening is not observed. Thus, the pearlite hardens more effectively, leading to a smaller zone of gross shear deformation, smaller total crack length, and better wear properties. The bainite, where the carbide morphology is intermediate between that of pearlite or tempered martensite, gives an intermediate wear performance.

5.0 SUMMARY AND CONCLUSIONS

1. In the hardness range, HRC 38-45, the wear rate depends strongly on initial hardness for tempered martensite, moderately so for bainite and very little, if at all, for pearlite. Lower wear rates are obtained for all pearlites than for tempered martensite or bainite of hardness, HRC 45. The dry wear rates of low rails are significantly less than those for corresponding high rails. Their dependence on hardness is relatively small.

2. Lubrication, particularly with pure grease, decreases the wear rates of high rails very significantly, but has a lesser effect for low rails. In general, little correlation exists between lubricated wear rates and either hardness or microstructure, however, the wear rate of pearlite appears to increase with increasing hardness.

3. A highly sheared layer is produced at the worn surface, whose depth is a maximum (> 250 μm) at the gauge corner. High microhardness values are obtained at and within 50 μm of the worn surface, particularly in dry wear. The hardest values occur at the surface of the gauge corner and for pearlite. These microhardness values, rather than the initial hardness of the steel, appear to control dry wear resistance.

4. Surface and subsurface cracks occur in the deformed shear zone and are intimately associated with inclusions, particularly MnS.

5. TEM examination of worn surfaces shows as considerable refinement of the intercarbide spacing, especially for pearlite, and the formation of very fine, polycrystalline ferrite grains. Diffraction patterns show that a strong possibility exists of texture formation.

On the basis of the above results it appears that pearlite of hardness HRC 38-40, is the optimum microstructure for this steel. Lowering the sulphur content should markedly lower the dry wear rate and this aspect is being investigated. All wear rates decrease drastically under lubrication to insignificant values. With the present test conditions, deep contact fatigue cracks or severe shells were not obtained, but their possibility of occurring does exist with longer lubricated testing.

6.0 REFERENCES

1. Stone, D.H. "The increasing demands on the servicability of rail steels". Canadian Metallurgical Quarterly 21(1), 1982, pp. 17-24.

2. Kalousek, J.
Bethune, A.E.
"Rail wear under heavy traffic conditions". In Rail Steels, Development, Processing and Use, ASTM STP 644, Philadelphia, Pa., 1978, pp. 63-79.

3. Gardiner et al.
"Evaluation of premium rail on 8° curves in the B.C. south line".
CN Rail Research Centre Report 152, St. Laurent, Quebec, 1979.

4. Bramwell, S.
McElroy, T.F.
"Twenty-five years of heavy axle load unit train operation on the QNSL railway".
In 1st International Heavy Haul Railways Conference Proceedings, Perth, Australia, Paper A4, Sept. 1978.

5.
"United States Steel (1975) Railroad Facts".
Technical report no. 3.

6. Gino, T.
Gocho, M.
"Rail production at number 2 large section mill at the Fukuyama Works".
Iron and Steel Engineers, Vol. 52., June 1975, pp. 25-31.

7. Ichinose, H. et al.
"High strength rails produced by two stage flame heating and slack-quenching".
In Second International Heavy Haul Railways Conference Proceedings, Paper 82-HH-19, Colorado Springs, USA, 1982, pp. 178-186.

8. Marich, S.
Curcio, P.
"Development of high strength alloyed rail steels suitable for heavy duty applications".
In Rail Steels, Development, Processing and Use, ASTM STP 644, Philadelphia, Pa., 1978, pp. 167-198.

9. Smith, Y.E.
Fletcher, F.B.
"Alloy steels for high-strength as-rolled rails".
Ibid, pp. 212-232.

10.
"Vanadium in rail steels: proceedings of a seminar in Chicago".
VANITEC, Nov. 1979. See papers by H. Schmedders, p. 3; A.M. Sage et al., p. 12; S. Marich, p. 23; F.B. Fletcher et al., p. 41; P. Dilewijns et al., p. 48.

11. Roney, M.D.
"Economic aspects of the wear of rail on Canadian systems".
In Contact Mechanics and Wear of Rail/Wheel Systems, Kalousek/Dukkipati/Gladwell (eds.), University of Waterloo Press, 1983, pp. 271-281.

12. Steele, R.K. "Perspectival review of rail behaviour at the FAST".
Canadian Metallurgical Quarterly 22(3), 1983, pp. 353-367.

13. Hodgson, W.H. et al. "The development of a second generation of alloy steel rails for heavy haul applications.
2nd International Heavy Haul Railway Conference Proceedings, Colorado Springs, 1982, pp. 207-215.

14. Koerfer, E. Written discussion to paper in Ref. 8 p. 202.

15. Masumoto, H. et al. "Development of wear resistant and anti-shelling high strength rail in Japan".
In 1st International heavy Haul Railways Conference Proceedings".
Perth, Australia, Session 212, Paper H.1.

16. Ichinoise, H. et al. "An investigation on contact fatigue and wear resistance behaviour in rail steels".
Ibid., Session 307, Paper I.3.

17. Bradley, J.
Kalousek, J. "Modelling of roller rig contact forces for three-point contact based on Kalker's simplified non-linear creep theory for single point contact".
NRC Report LTR-WE-29, Sept. 1982.

18. Kalousek, J. "Development of a dual disc on disc rail/wheel wear testing facility".
In Canadian Metallurgical Quarterly 21(1), 1982, pp. 67-72.

19. Fegredo, D.M. et al. "The development of very hard and strong premium rail by controlled cooling procedures".
In Canadian Metallurgical Quarterly 22(3), 1983, pp. 385-395.

20. Kalousek, J.
Rosval, G. "Lateral creepage and its effect on wear in rail wheel interface".
In Contact Mechanics and Wear of Rail/Wheel Systems, Kalousek, Dukkipati and Gladwell (eds.), University of Waterloo Press, 1982.

21. Ghonem, H.
Kalousek, J.
Stone, D.H.
Dibble, D.W. "Observations of rail wear on heavy haul railway lines,".
In Contact mechanics and Wear of Rail/Wheel Systems, Kalousek, Dukkipati and Gladwell (eds.), University of Waterloo Press, 1982.

22. Underwood, E.E. "Application of quantitative metallography". In Metals Handbook, Vol. 8, 8th edition, ASM, 1973.

23. Kalousek, J. "Wear and lubrication effect on subsurface failure of several steels". Submitted to the 11th Leeds-Lyon Symposium on Tribology: Mixed Lubrication and Lubricated Wear.

24. Steele, R.K. "Rail: its behaviour and relationship to total system wear". Second International Heavy Haul Railway Conference Proceedings, Colorado Springs, 1982, Paper 82-HH-24, pp. 227-276.

25. Johnson, K.L. Jeffries, J.A. "Plastic flow and residual stresses in rolling and sliding contacts". In Symposium on Fatigue in Rolling Rolling Contact, Paper 5, Institute of Mechanical Engineers, London, 1963, pp. 50-61.

26. Beagley, T.M. "Severe wear of rolling/sliding contacts". Wear, 36, 1976, pp. 317-335.

27. Bolton, P.J. Clayton, P. "Rolling-sliding wear damage in rail and tyre steels". Wear, 93(2), 1984, pp. 145-165.

28. Langford, G. Metallurgical Transactions A, 8A, 1977, pp. 861-875.

TABLE 1

Summary of Materials and Test Sequences

Specimen Code	Microstructure	Approx. Hardness (HRC)	Type of Test
A-HR (high rail) -LR (low rail)	Tempered Martensite	38	Full sequence (2,400,000 revs.)
B-HR -LR	"	42	" "
C-HR LR	"	45	" "
D-HR -LR	Bainite	38	Full sequence (2,400,000 revs.)
E-HR -LR	"	42	" "
F-HR -LR	"	45	" "
G-HR -LR	Pearlite	38	Full sequence (2,400,000 revs.)
H-HR -LR	"	42	" "
I-HR -LR	"	45	" "
J-HR -LR	Pearlite	38	Dry (80,000 revs.)
K-HR -LR	Tempered Martensite	38	Dry (80,000 revs.)

TABLE 2

Approximate depth (μm) of grossly deformed shear zone in high rails from the worn surface to where the grains become just recognisable

Disk	Centre of Gauge Face	Centre of Gauge Corner	Junction of Running Surface & Gauge Corner	Centre of Running Surface	Junction of Running Surface & Field Corner
A-HR	25	270	250	70	0
B-HR	25	225	250	40	0
C-HR	15	315	340	50	0
D-HR	25	450	450	55	10
E-HR	25	280	405	55	0
F-HR	15	270	180	55	0
G-HR	40	260	295	80	0
H-HR	45	205	215	55	10
I-HR	35	150	160	45	0
J-HR	25	280	295	75	0
K-HR	25	495	675	235	0

TABLE 3

Hardness (HV_{100}) at various depths (μm) below the worn surface for low rail discs

Hardness at centre of running surface for 0-250 μm depths

Disk	0	5	10	15	25	50	250
A-LR	540	540	540	540	480	405	351
C-LR	590	579	608	590	590	437	433
D-LR	530	510	490	480	450	394	376
F-LR	530	530	530	490	460	387	370
G-LR	608	590	579	579	450	425	370
I-LR	560	579	579	560	540	405	345
J-LR	620	572	623	604	509	441	371
K-LR	627	567	528	539	538	442	360

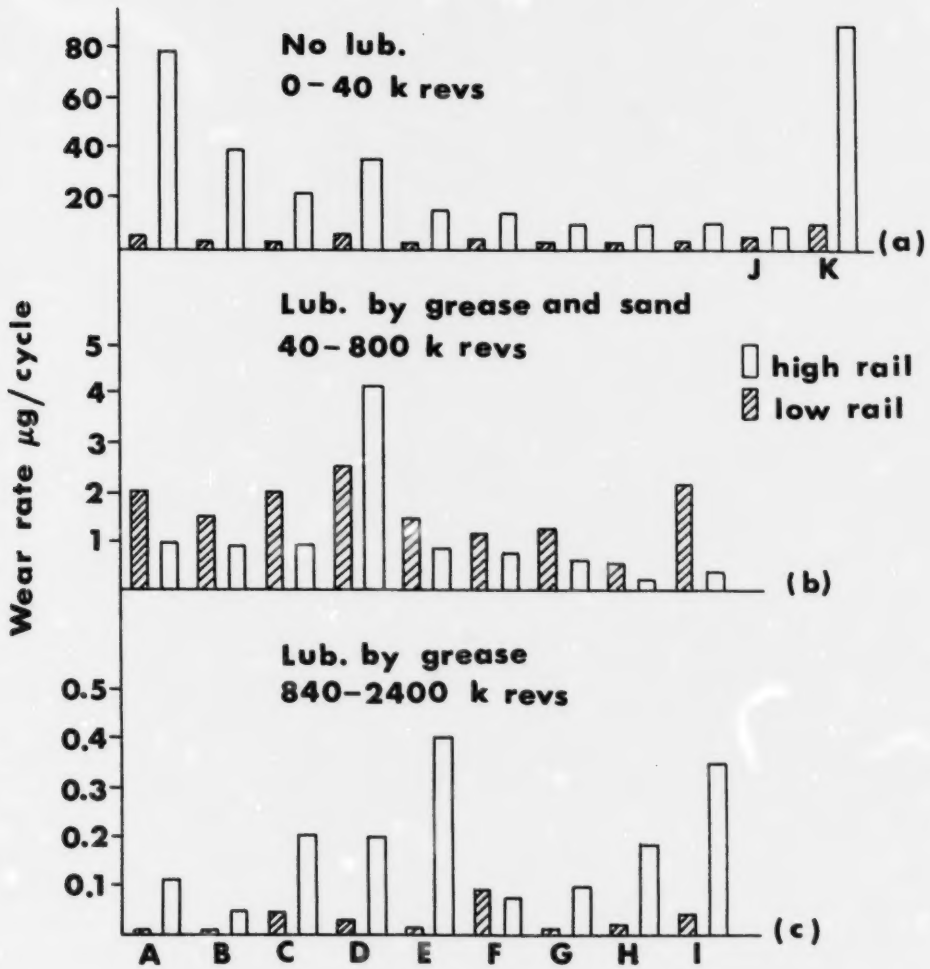

Fig. 1. Wear rates observed: (a) no lubrication; (b) grease/20% sand lubrication; (c) pure grease lubrication. Note scale changes in a, b and c.

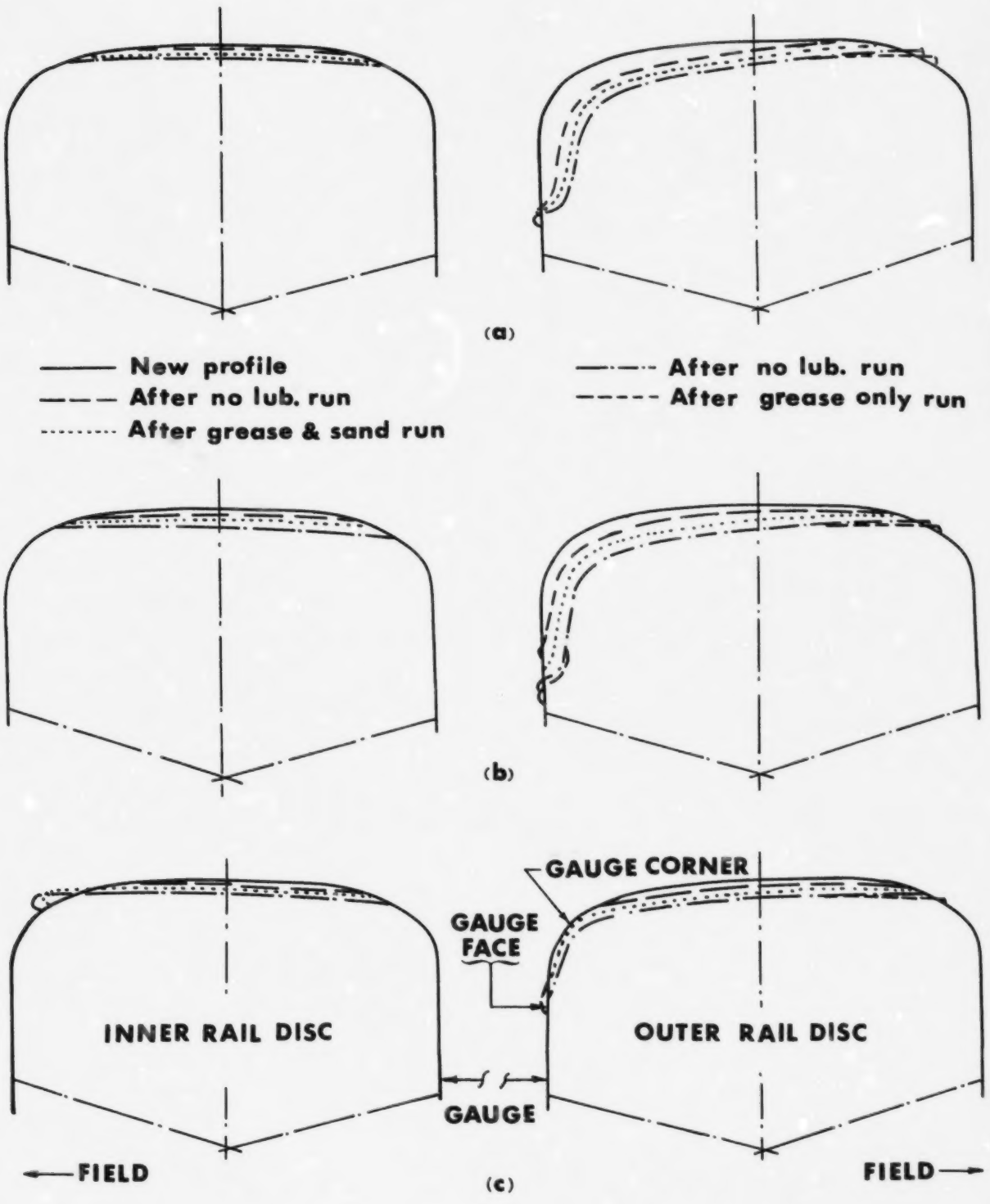

Fig. 2. Wear profiles after each of the four test stages: (a) disks A, tempered martensite; (b) disks D, bainite; (c) disks G, pearlite.

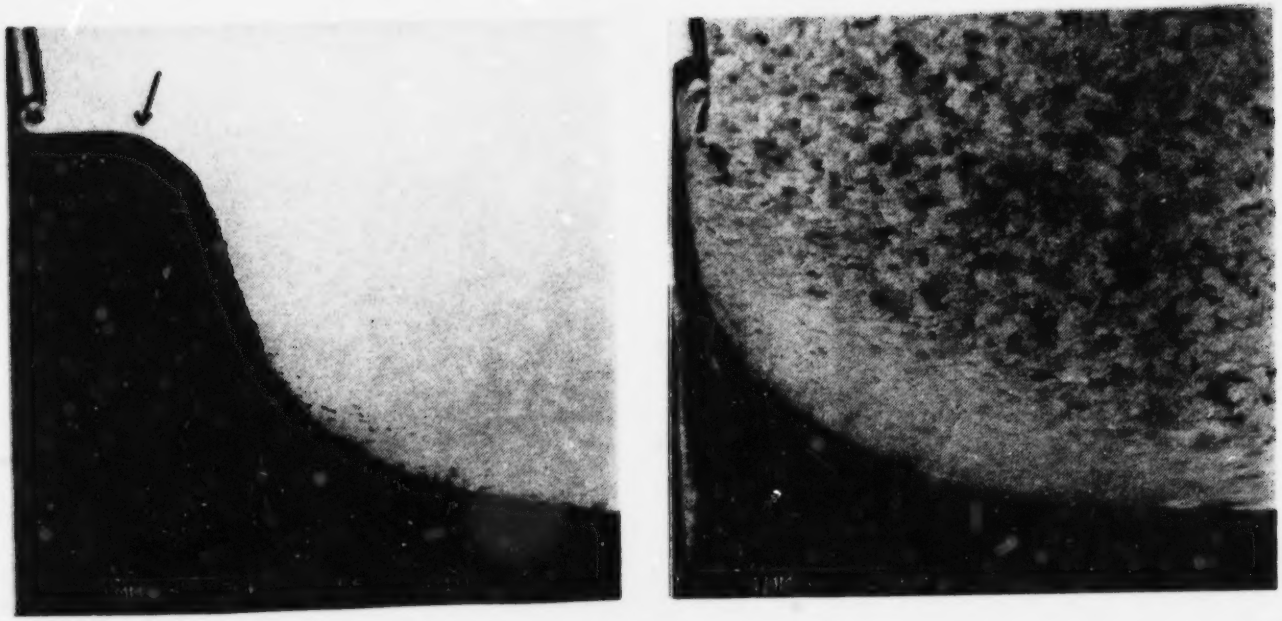

(a) (b)

Fig. 3: Gauge corner and gauge face wear after two periods of dry wear resulting in development of shoulder (a) or shear lip (b): (a) disk K-HR, tempered martensite; (b) disk J-HR, pearlite.

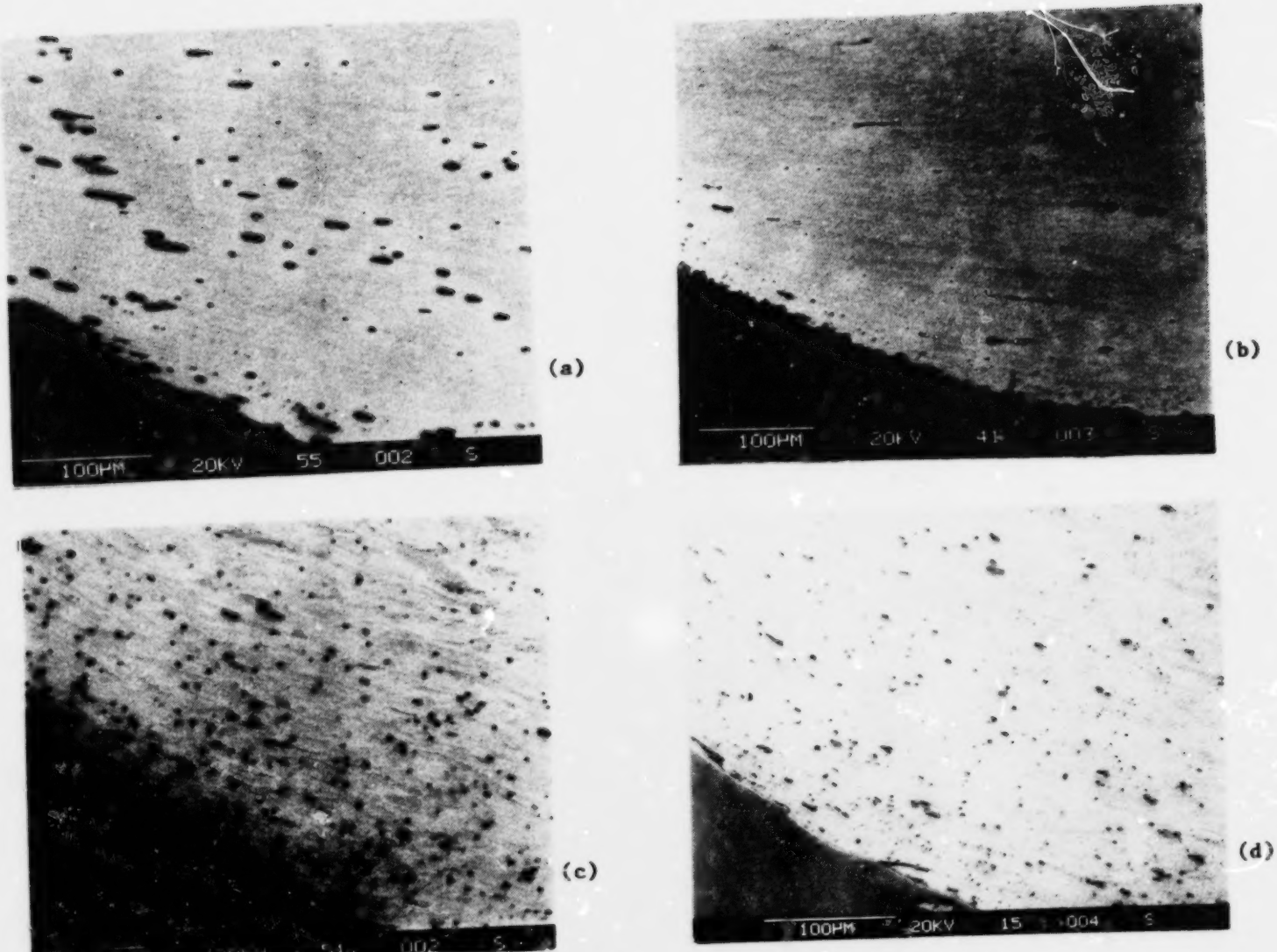

Fig. 4: Gauge corner deformation with surface and subsurface cracks: (a) disk K-HR; (b) disk A-HR; (c) disk J-HR; (d) disk G-HR

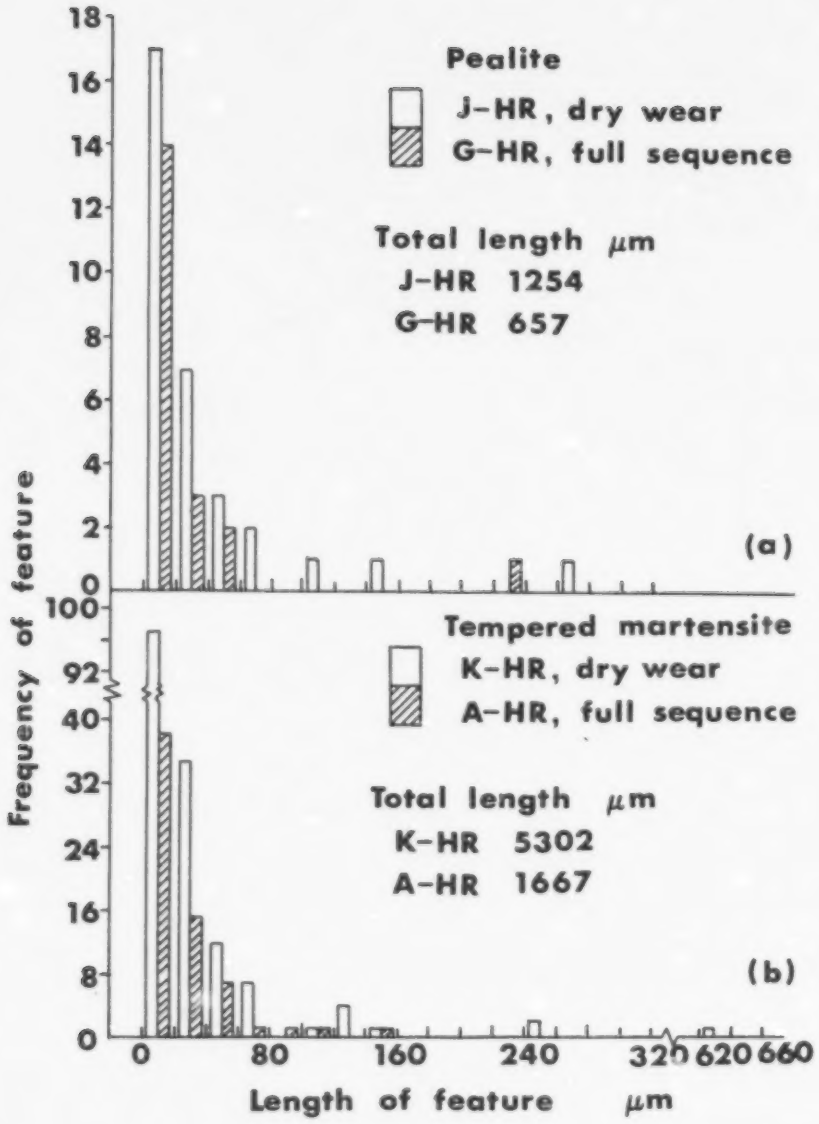

Fig. 5. Crack frequency vs. length, image analyser data.

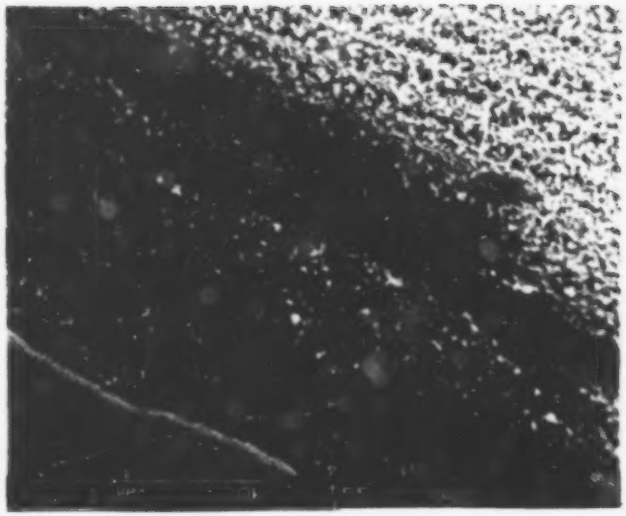

(a)

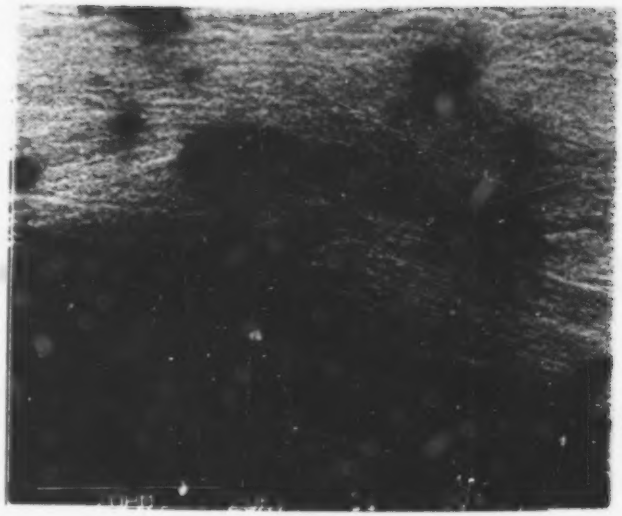

(b)

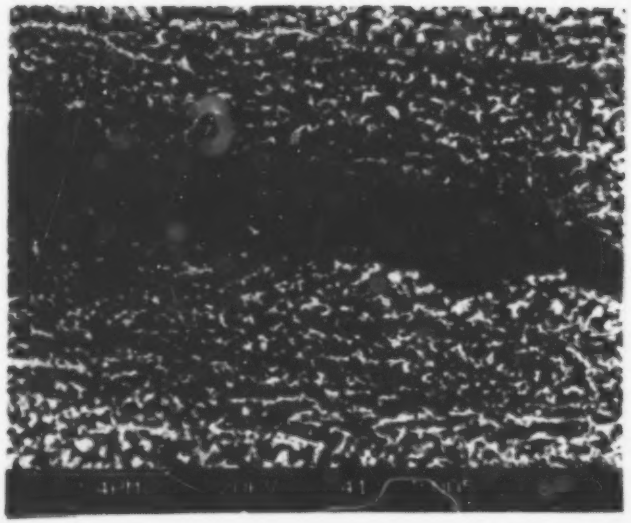

(c)

Fig. 6: Association of cracks with inclusions: (a) disk K-HR, MnS inclusions; (b) disk J-HR, MnS inclusions; (c) disk A-HR, undeformed oxide inclusions.

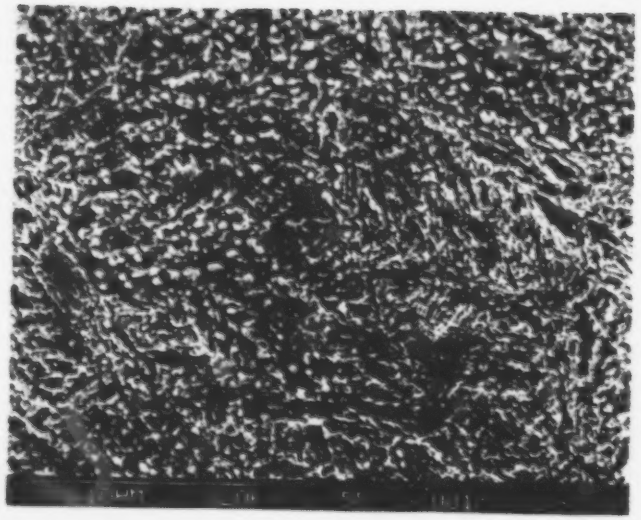

(a)

(b)

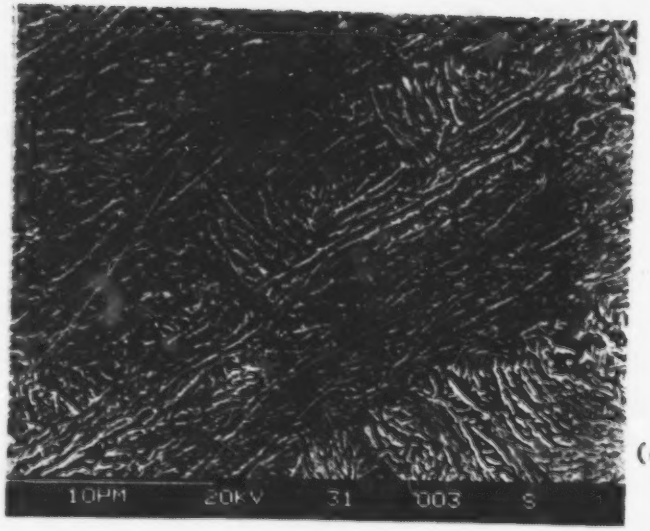

(c)

Fig. 7: Undeformed microstructures: (a) tempered martensite (disk K-HR); (b) pearlite (disk G-HR); (c) bainite (disk D-HR).

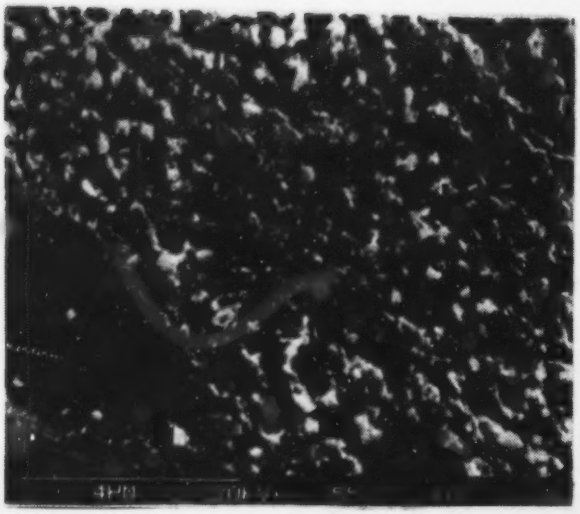

(a)

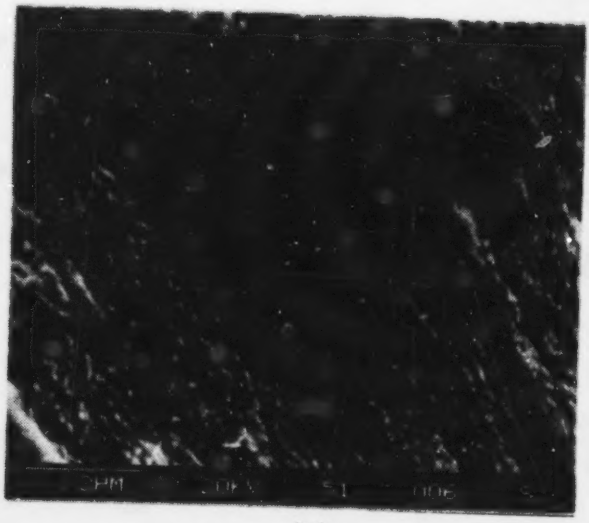

(b)

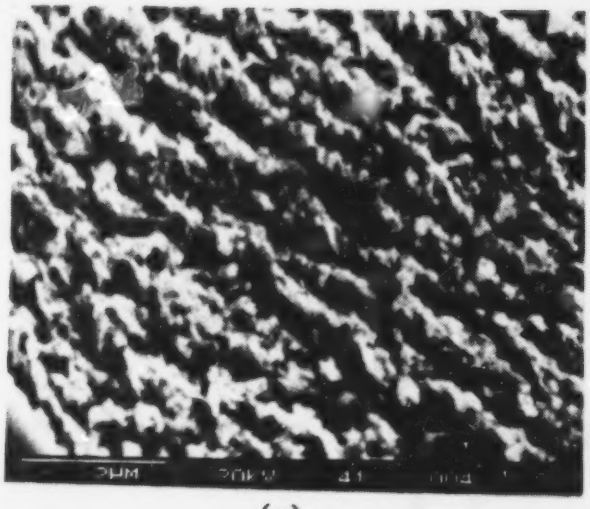

(c)

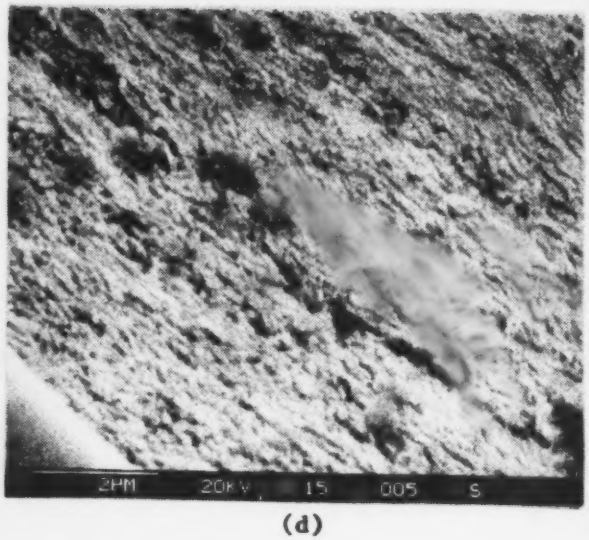

(d)

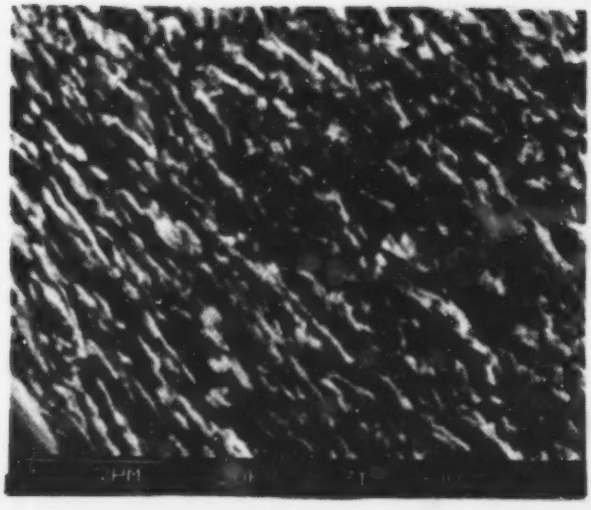

(e)

Fig. 8: Worn near-surface microstructure: (a) disk K-HR, tempered martensite, dry wear; (b) disk J-HR, pearlite, dry wear; (c) disk A-HR, tempered martensite, full sequence; (d) disk G-HR, pearlite, full sequence; (e) disk D-HR, bainite, full sequence.

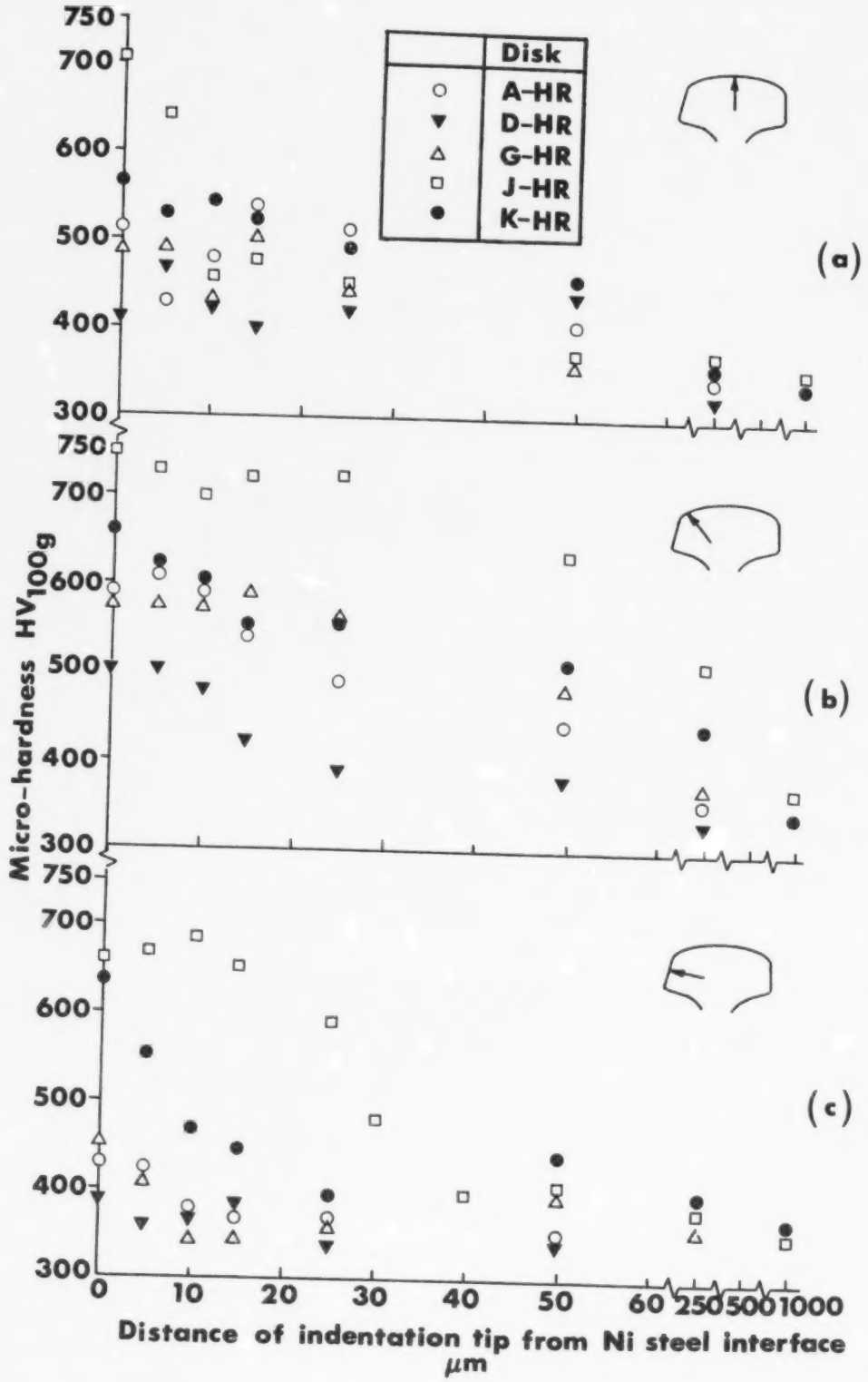

Fig. 9. Typical microhardness traverses at the centre of: (a) running surface; (b) gauge corner; (c) gauge face.

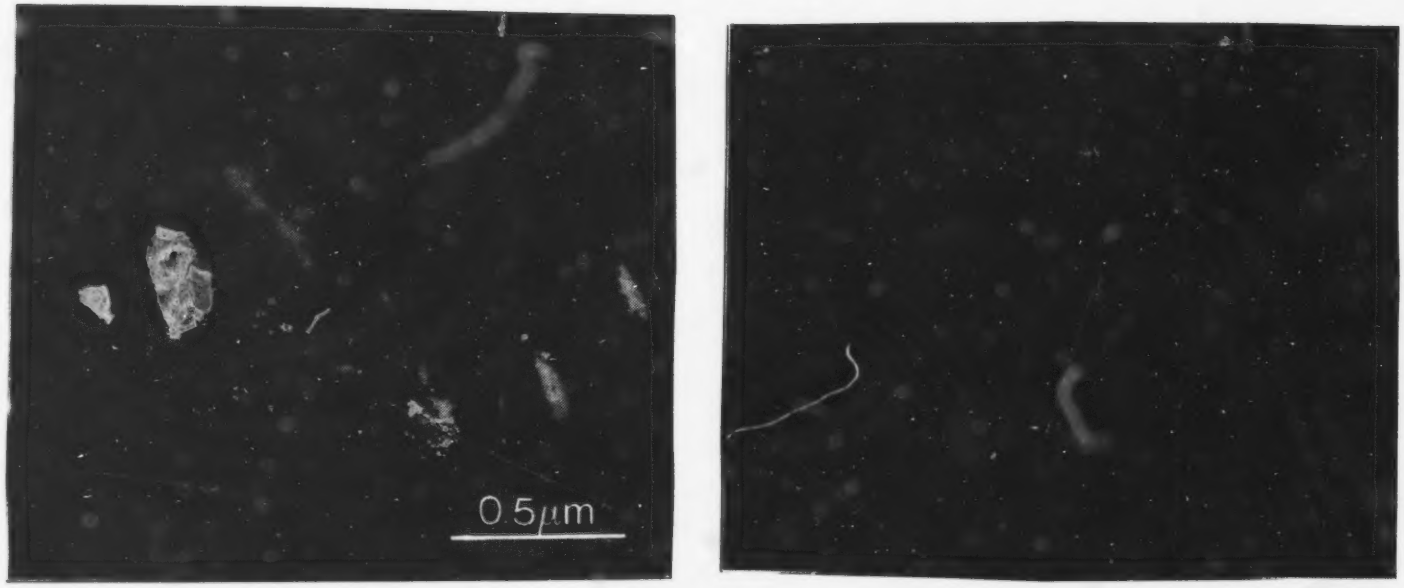

(a) (b)

Fig. 11: (a) Disk H-HR, 30 μm below running surface. TEM, Thinned foil; (b) diffraction pattern corresponding to (a)

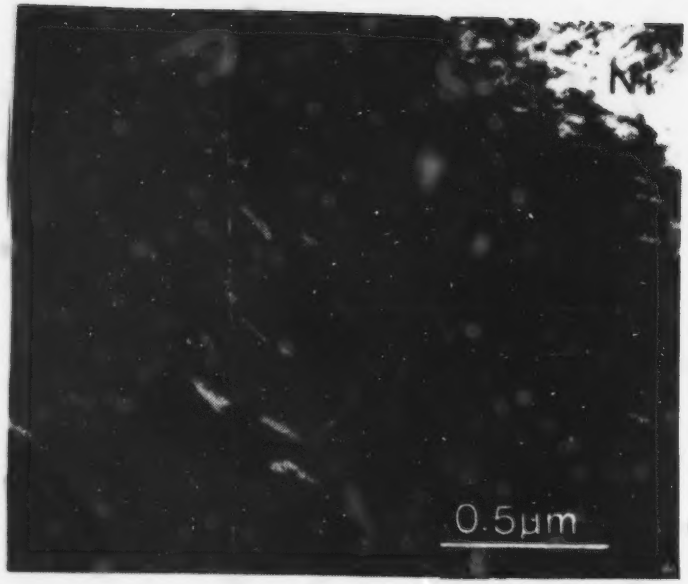

(a)

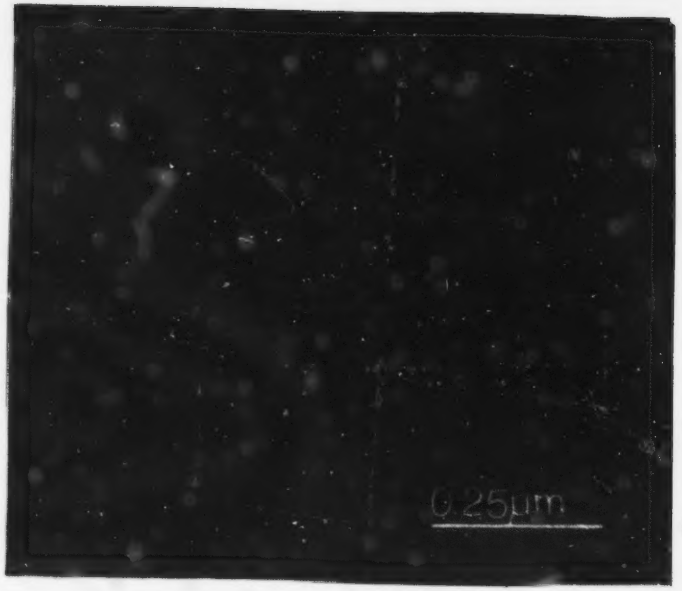

(b)

(c)

Fig. 12: Disk E-HR, between gauge corner and centre of running surface. TEM, thinned foil, (a) bright field; (b) dark field, {110} reflection; (c) diffraction pattern.

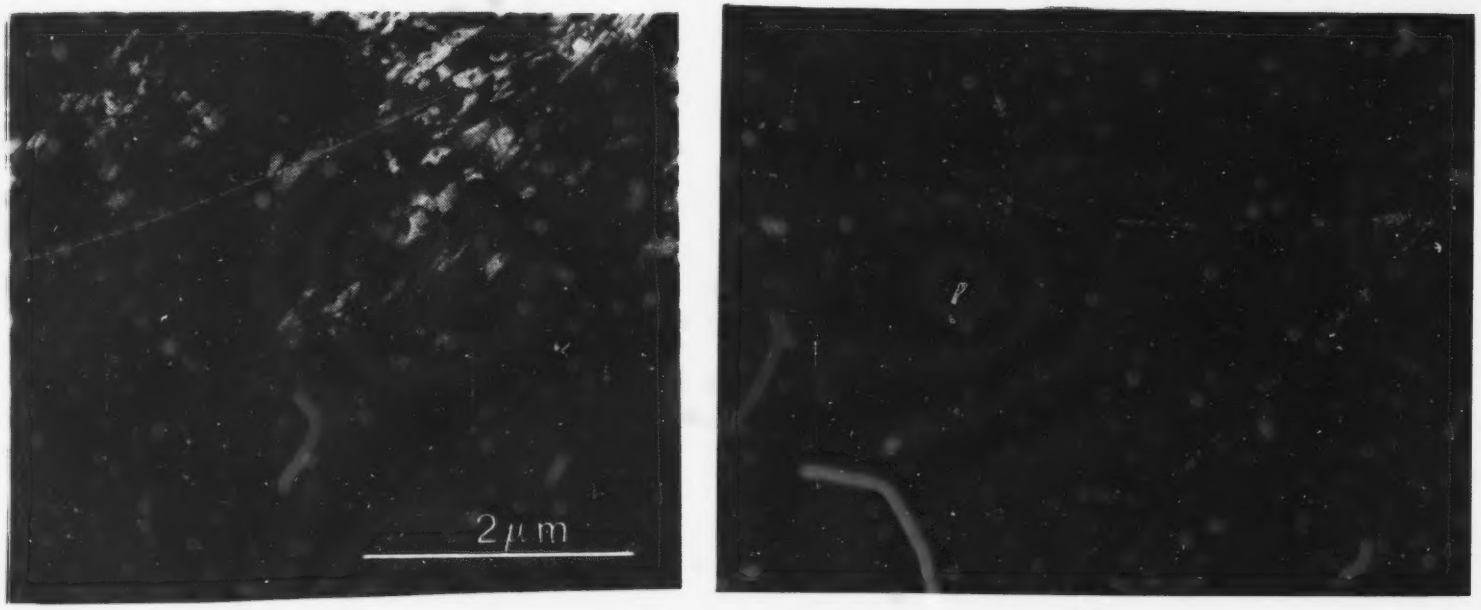

(a) (b)

Fig. 13: (a) Disk A-HR, 70 μm below running surface. TEM, thinned foil. (b) Diffraction pattern corresponding to (a).

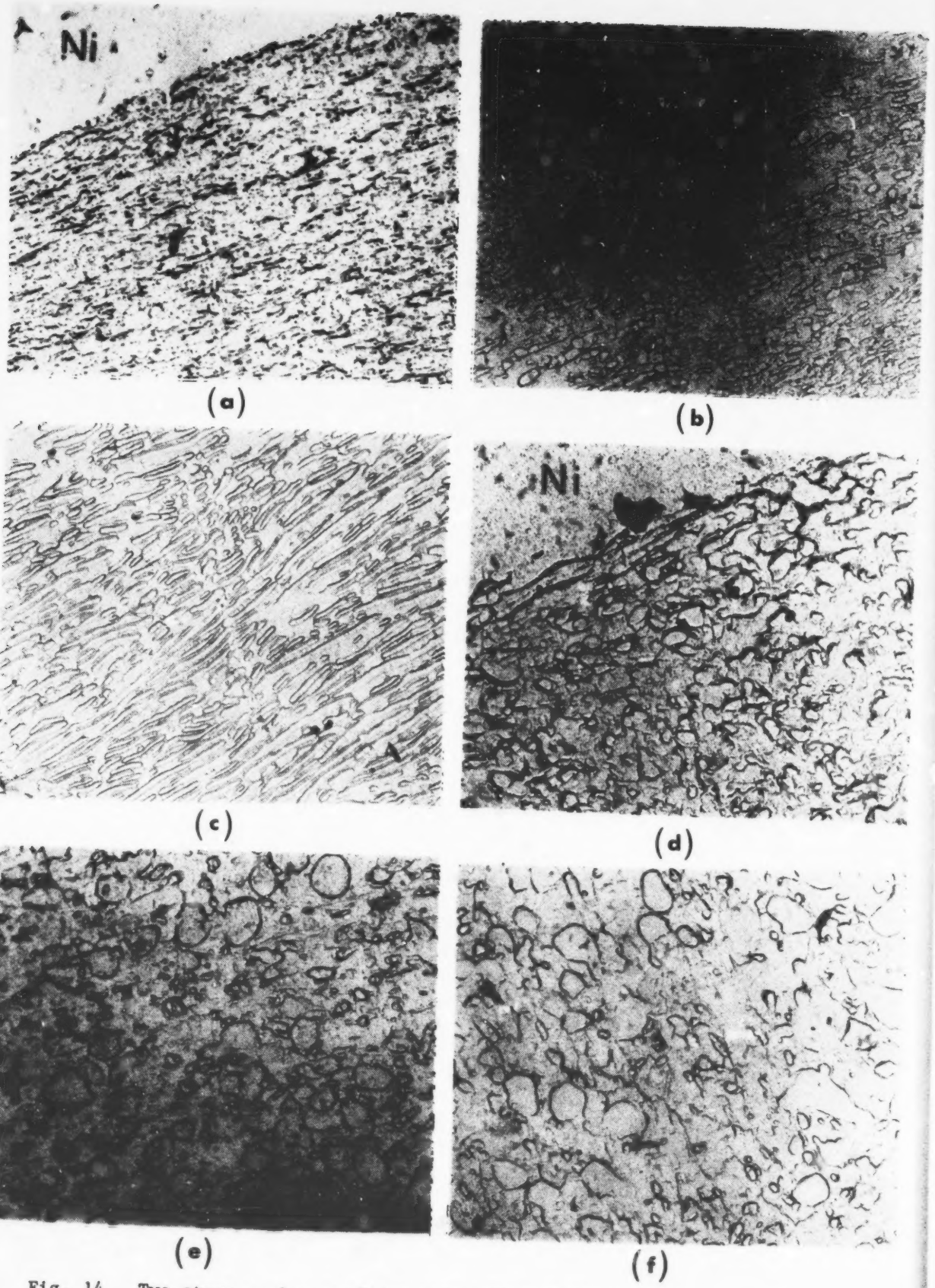

Fig. 14. Two stage carbon replica, TEM: Disk J-HR, (a) gauge corner surface, (b) 50 μm and (c) 500 μm below surface; Disk K-HR (d) gauge corner surface, (e) 50 μm and (f) 500 μm below surface.

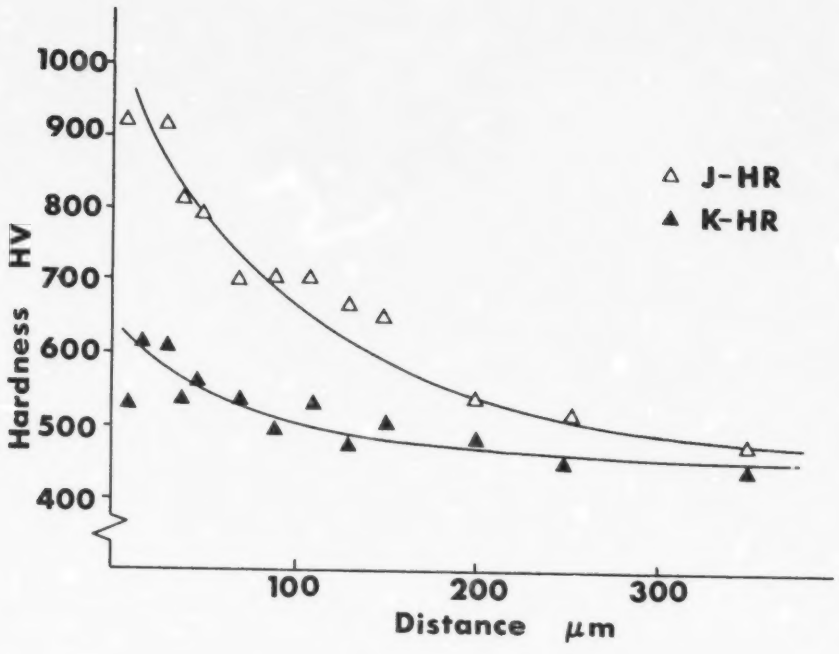

Fig. 10. Gauge corner microhardness traverses, samples J-HR and K-HR.

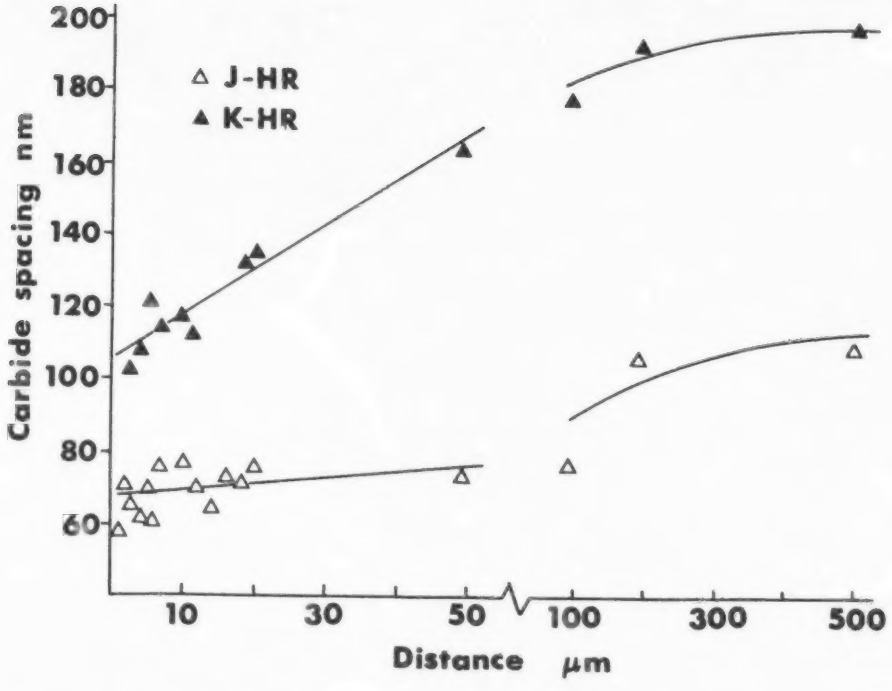

Fig. 15. Inter-carbide spacing vs. depth below gauge corner surface (J-HR and K-HR).

PART III

EXAMINATION OF RAIL WEAR DEBRIS

EXAMINATION OF RAIL WEAR DEBRIS

1.0 INTRODUCTION

During 1983/84, an examination of fine rail wear debris particles was undertaken. Many of these particles were so-called "white-etching" particles, and it had been suspected that some of these might consist of cementite. Relatively few of these particles were successfully identified, but none consisted of massive cementite. The work is reported in [Ref. 1]. The present work was undertaken as a continuation of the earlier project. A number of relatively large rail (or wheel) wear debris particles were received for examination. Any which were wholly or partly "white etching" in character would be of particular interest.

2.0 EXPERIMENTAL

2.1 Sample Preparation - TEM

Some forty odd particles were received. They were arbitrarily numbered and then photographed. Transmission electron microscope (TEM) samples were prepared by the standard technique of sectioning, disc cutting, hand grinding and final thinning in a twin-jet electropolishing cell, using an electrolyte consisting of:

225 ml methanol

45 ml butyl cellusolve

30 ml perchloric acid

Most samples were cut from the particles as received. These samples are parallel to the broad face of the particles from which they were cut, and the running direction of the wheel will lie in the plane of the micrographs. Some of the smaller particles were first electroplated with nickel, and TEM samples prepared perpendicular to the running surface. Such samples are indicated by the letter "P" following the number. The electroplating technique consisted of a thorough degreasing in organic solvents, followed by plating in a bath consisting of:

150 g $NiCl_2 \cdot 6H_2O$

19 g H_3BO_3

0.25 g sodium lauryl sulfate

H_2O to make 500 ml

2.2 Phase Identification

Phases were identified or sought using transmission electron diffraction. The three phases of interest were ferrite, martensite and cementite. Ferrite is b.c.c., a = 0.2861 nm. Martensite is a distorted ferrite, described as b.c.t. The lattice constants a and c depend on the carbon content, and for eutectoid steel, with 0.8% C, they are:

a = 0.2851 nm

c = 0.2954 nm

Cementite is orthorhombic, with

a = 0.4528 nm

b = 0.5092 nm

c = 0.6796 nm

TABLE 1: Expected Diffraction Pattern

FERRITE		MARTENSITE		CEMENTITE	
h,k,l	D, mm	h,k,l	D,mm	h,k,l	D,mm
110	46.5	101	45.9	112	39.5
		110	46.7	200	41.6
200	65.8	002	63.7	120	42.8
		200	66.0	121	44.8
211	80.5	112	79.0	210	45.7
		211	80.4	022	46.6
220	93.0	202	91.7	103	46.8
		220	93.3	211	47.8
310	104.0	103	101.1	113	50.3
		301	104.0	122	50.8
		310	104.3	212	53.4
222	113.9	222	113.0		

The principal reflections from these phases are summarized in Table 1. Here, "D" is the diameter of the expected diffraction ring, at the typical magnification of the diffraction patterns as presented in this report, although there is some variation in magnification between photographs. The effect of the distortion of the ferrite to martensite is to cause most of the ferrite diffraction lines to be split into groups of two or three. If these groups can be resolved, a distinction can be made between martensite and ferrite. By inspection of the diffraction pattern, it can be seen that the best diffraction ring to distinguish between martensite and ferrite would be the $\{200\}$ ring. Unfortunately, this ring is often incomplete. The $\{110\}$ ring cannot be used because of the limited splitting and possible interference from cementite. The next three rings are progressively weaker and not widely split. Thus, electron diffraction, with our TEM, is not suitable for distinguishing between martensite and ferrite. However, high carbon martensite is usually heavily twinned, and may be recognized by this fact.

No conclusive evidence of martensite was found in the samples examined. On the other hand, the diffraction pattern of cementite is quite different from that of ferrite, and single crystal patterns, as from small individual grains, are even more distinctive. Thus, electron diffraction can unambiguously distinguish between ferrite and cementite. Note also in passing that the strong cementite reflections {210}, {022} and {103} would interfere with the {110} and {101} reflections of martensite or the {110} ferrite, so that the distinction between martensite and ferrite is even more difficult in the presence of cementite.

2.3 Optical Metallography

Samples were mounted, ground and polished using standard techniques, and etched in nital.

3.0 OBSERVATIONS

In this section are described typical micrographs of the samples examined.

3.1 Sample K-1

Figures 1-4 show the flake designated K-1. As shown in Figure 1, the original flake was about 6 mm × 28 mm. Figure 2 shows a microstructure of deformed ferrite-pearlite, suggesting the flake may have come from a wheel (hypoeutectoid) rather than a rail (eutectoid). Figure 3(a) shows a clear area of the sample, and the selected area diffraction pattern of Figure 3(b) identifies this as ferrite. The relatively complete rings, especially the {110} ring, show that the grain size is quite fine, much finer than 3.5 μm, the diameter of selected area. Figure 4(a) shows another region of this sample. Here we have pearlite, with a spacing of about 140 nm. There is quite a high dislocation density, and the diffraction pattern shows that the ferrite here is nearly monocrystalline, but with a half dozen or so subgrains over the 3.5 μm selected area. The microhardness of this sample was 465 HK.

3.2 Sample K-3

Figure 5 is a macro photo of sample K-3 (cm scale). Figure 6, at 500 X, shows that the sample would be considered light etching or perhaps white etching. Figure 7 shows the microstructure as seen by the TEM. Figures 7(a) and (b) show a fine grained ferrite-cementite mixture. There is no suggestion of the lamellar microstructure of pearlite, rather, the microstructure resembles a deformed tempered martensite. The fine grain size is shown more graphically in [Fig. 7c]. Here, individual white (or light) regions are separate grains. Grains ranging from about 80 nm to 500 nm diameter are seen. Flake K-3 thus is most likely a region transformed to martensite, e.g., due to wheel spinning, and subsequently tempered, as by subsequent, less intense, frictional heating. Sample K-3 had a microhardness of 470 HK.

3.3 Sample K-6

Figures 8 and 9 are macro and optical micrographs of sample K-6. The "bumps" in the micrograph reappeared after repolishing and re-etching thus, we believe them to be real, and not any polishing artifact. They are not identified. The sample would be classified as light etching. However, [Fig. 10a] shows pearlite with a spacing of about 93 nm. The rings in the diffraction pattern show that the sample is fine grained, i.e., many grains are contained in the field shown in [Fig. 10a], although the cementite lamellae are straight and continuous giving the misleading impression of a monocrystalline ferrite, or undeformed pearlite colony. The high dislocation density and very fine pearlite spacing also suggest that a large amount of deformation has taken place. The sample had a microhardness of 490 HK.

3.4 Sample K11P

As shown in [Figs. 11 and 12], this sample would be considered white etching, except for a few dark stringers, almost certainly MnS. However, [Figs. 13 and 14] show that the microstructure is, in fact, very fine (100 nm) deformed pearlite. The microstructure is quite as one sees near the surface of worn rail [Ref. 2]. The microhardness of this sample was 430 HK.

3.5 Sample K18P

Figures 15 and 16 show optical macro and microphotographs of this sample. TEM micrographs [Figs. 17a, b and c] confirm that this sample is pearlite, of variable spacing. The hardness of sample K18 was 470 HK.

3.6 Sample K21

The sample is shown in [Fig. 18]. The micrograph, [Fig. 19], suggests that the sample would be classified as "white etching", but [Figs. 20-22] show pearlite, of a variable but very fine spacing, about 40 nm from [Fig. 21a], rather more in parts of [Fig. 22]. Corresponding to this fine spacing was quite a high hardness, of 540 HK.

3.7 Sample K40P

Figures 23-26 show sample K40P. No macrophoto was taken of this very small (mm size) flake. Figures 23 and 24 show aligned pearlite, and some evidence of deformation bands or crushing similar to K11P, or as has also been reported in [Ref. 2]. Figures 25 and 26 show the microstructure to consist of pearlite of very fine grain size. As for other samples, the fineness of the grain size is inferred from the continuity and smoothness of the diffraction rings. The pearlite spacing shown in [Fig. 26a] is about 45 nm. The microhardness of the sample was a very high 680 HK.

4.0 SUMMARY AND CONCLUSIONS

Of the seven debris or flake samples reported herein, two would be considered "white etching" except only for some MnS inclusions, and two "light etching". All samples were pearlitic, except K-1, which was ferrite-pearlite, and K3 which gave the appearance of tempered martensite. All had very fine grain size, micron and submicron in diameter. The microhardness values varied from a low of 430 HK for sample K11 (white etching) to 680 HK for sample K40 (fine pearlite, not white etching). It would appear that very fine pearlite may be relatively resistant to etching, and give the appearance of a white etching constituent, when etched for a time sufficient to darken a coarser pearlite. No evidence was found for massive cementite, or for "squeezing out" of ferrite between cementite laths. Rather, ferrite and cementite deformed together, much as shown by Langford [Ref. 3] in wire drawing experiments, to produce a pearlite spacing as fine as 40 nm. This is less than half the spacing seen in a very hard premium rail steel, and about one seventh that in a coarser standard eutectoid rail steel.

5.0 REFERENCES

1. Abraham, H.M. "Microscopic Examination and Identification of Rail/Wheel Wear Debris Particles". M.A.Sc. Thesis, Technical University of Nova Scotia, 1984.

2. Laufer, E.E. MacDonald, C. "Transmission Electron Microscopy Study on the Effects of Simulated Rail Loading on an Experimental Premium Rail Steel". CANMET Contract Report OSU81-00231, May 1985.

3. Langford, G. "Deformation of Pearlite". Metallurgical Transactions Abstract ,1977, pp. 861-875.

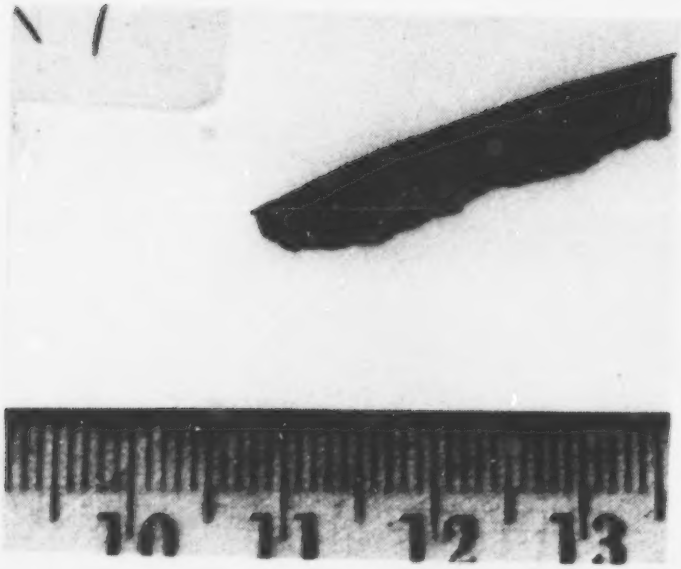

Figure 1: Macro Photo of K1 Flake, (Neg. 31B)

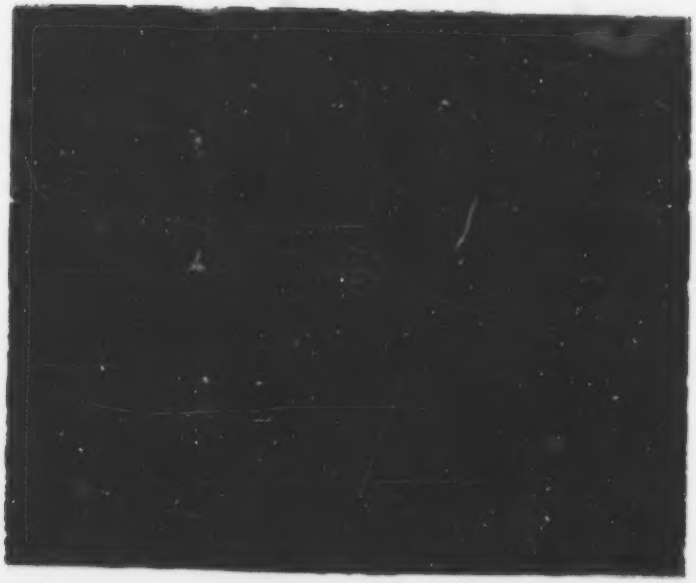

Figure 2: Optical Micrograph of K1 Flake, 1,000 × (Neg. 26KF)

Figure 3(a): Sample K1, 75,000 × (Neg. 3294)

Figure 3(b): Diffraction Pattern Corresponding to Figure 3(a), (Neg. 3295)

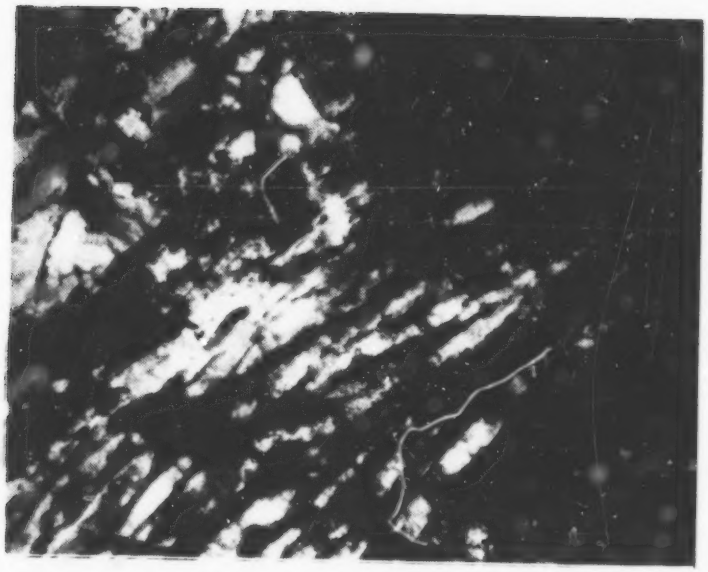

Figure 4(a): Sample K1, 25,000 × (Neg. 3296)

Figure 4(b): Diffraction Pattern Corresponding to Figure 4(a), (Neg. 3297)

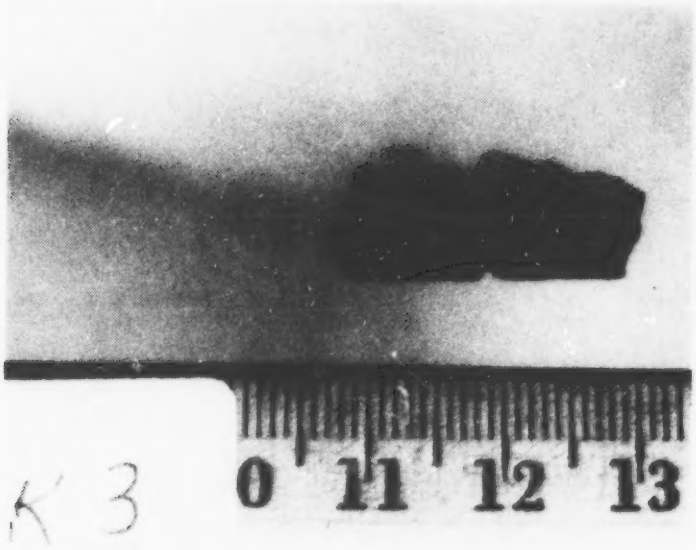

Figure 5: Macro Photo of K3 Flake (Neg. 20D)

Figure 6: Optical Micrograph of K3 Flake, 500 × (Neg. 17KF)

Figure 7a: Sample K3, 25,000 × (Neg. 3367)

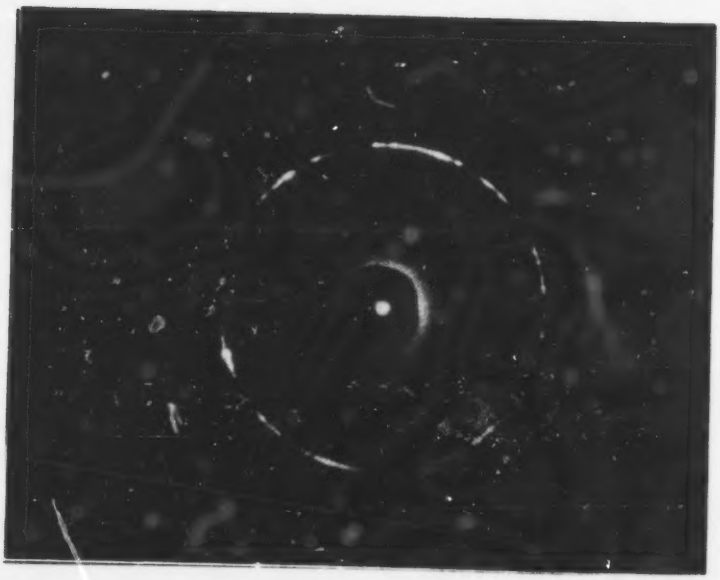

Figure 7b: Diffraction Pattern Corresponding to Figure 7a (Neg. 3368)

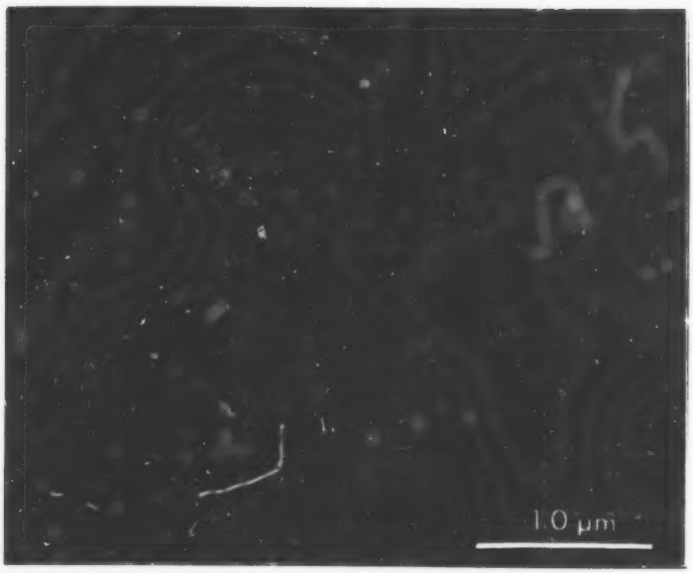

Figure 7c: Dark Field, same area as 7a, 110 Reflection, 25,000 × (Neg. 3369)

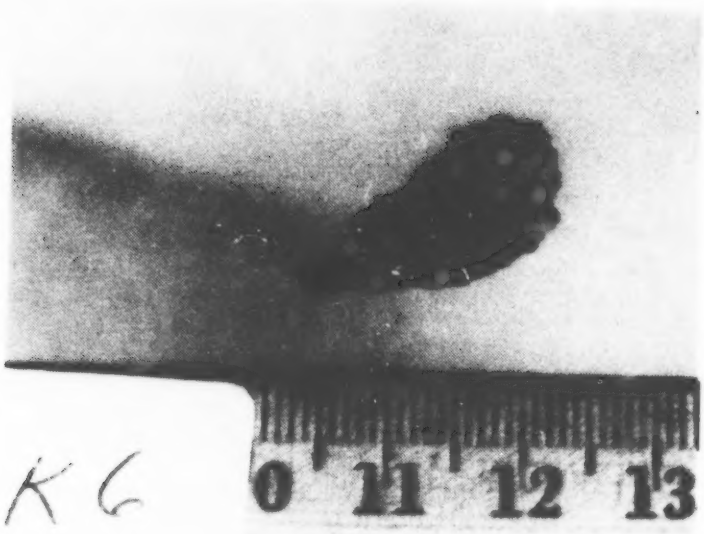

Figure 8: Macro Photo of K6 Flake (Neg. 26D)

Figure 9: Optical Micrograph, 500 × (Neg. 6KF)

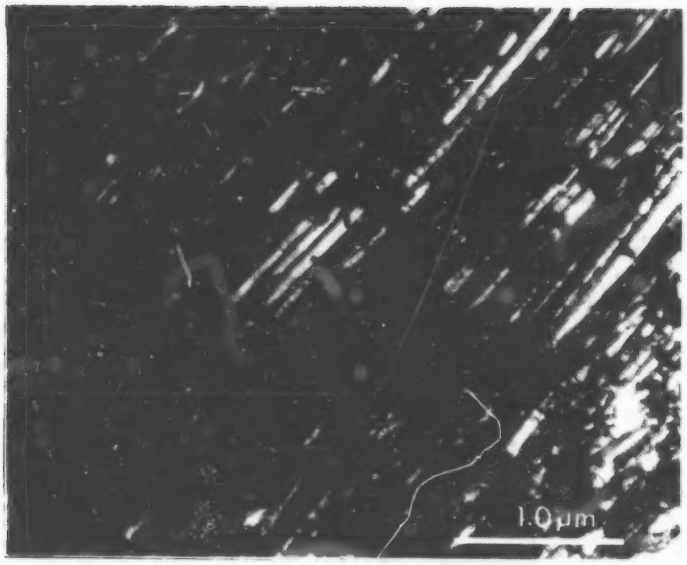

Figure 10a: Sample K6, 25,000 × (Neg. 3352)

Figure 10b: Diffraction Pattern Corresponding to Figure 10a (Neg. 3353)

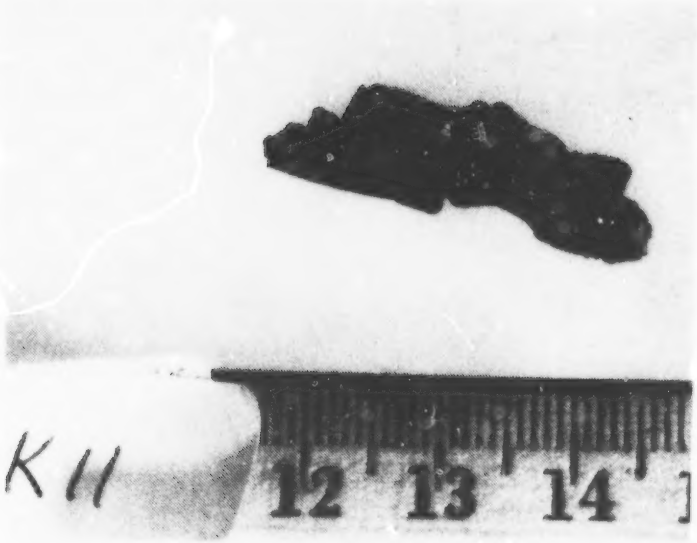

Figure 11: Macro Photo of K11P Flake (Neg. 35C)

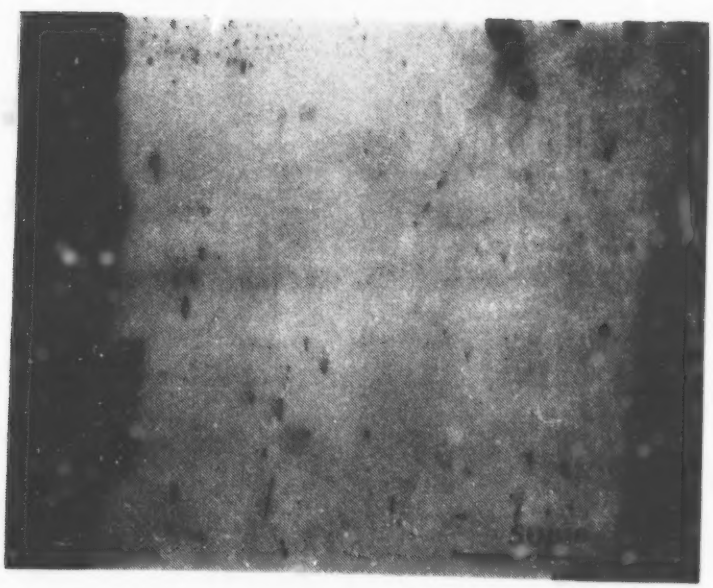

Figure 12: Optical Micrograph of K11P Flake, 500 × (Neg. 4KF)

Figure 13: Sample K11P, 25,000 × (Neg. 3358)

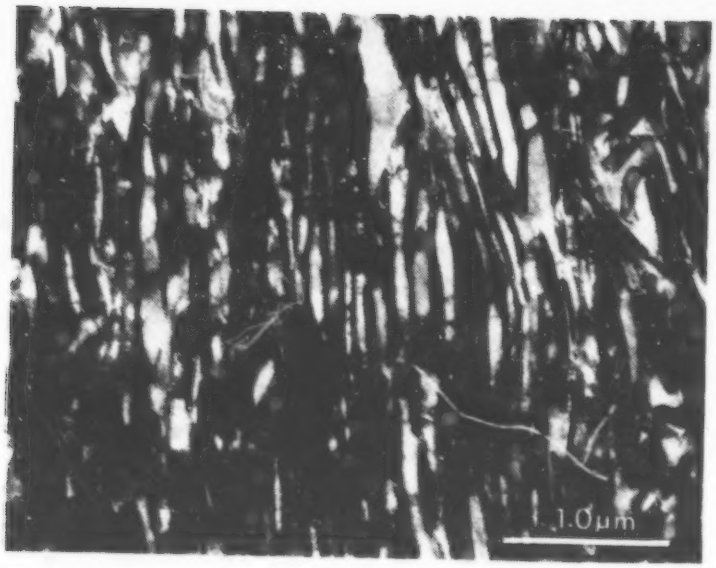

Figure 14a: Sample K11P, 25,000 × (Neg. 3362)

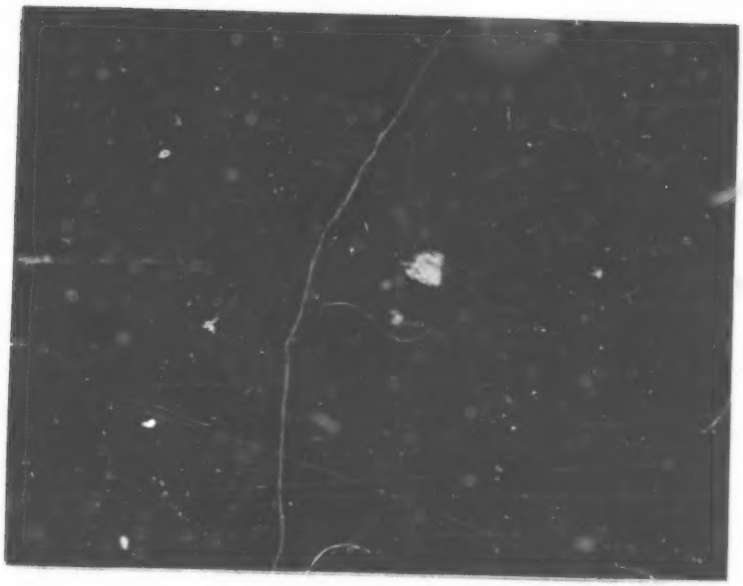

Figure 14b: Diffraction Pattern Corresponding to Figure 14a (Neg. 3363)

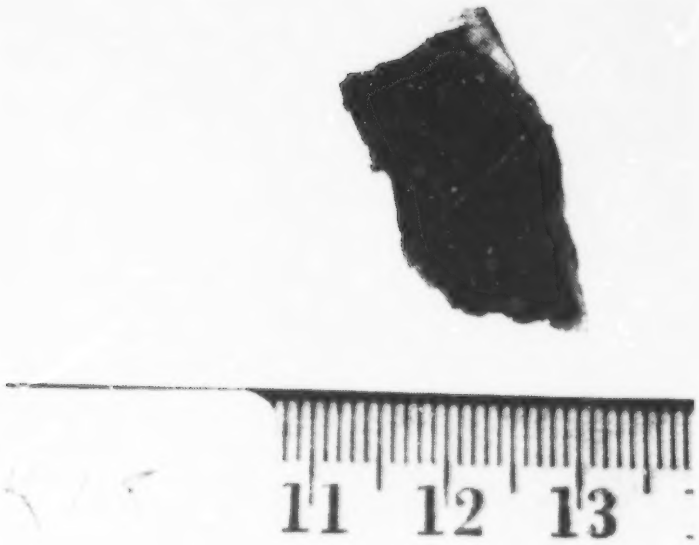

Figure 15: Macro Photo of K18P Flake (Neg. 4C)

Figure 16: Optical Micrograph of K18P Flake, 1,000 × (Neg. 50KF)

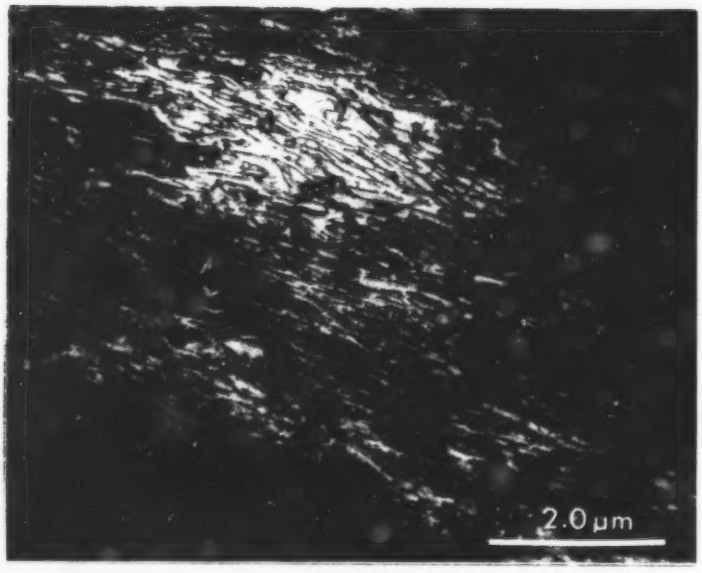

Figure 17a: Sample K18P, 6,000 × (Neg. 3242)

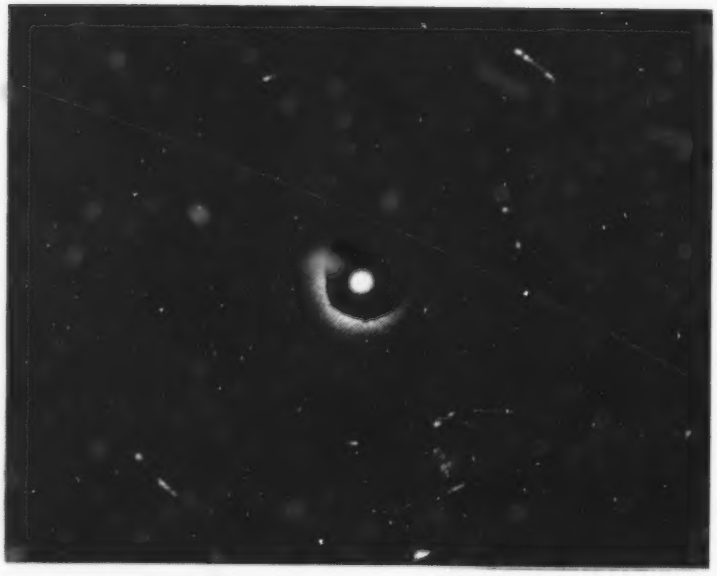

Figure 17b: Diffraction Pattern Corresponding to Figure 17a (Neg. 3244)

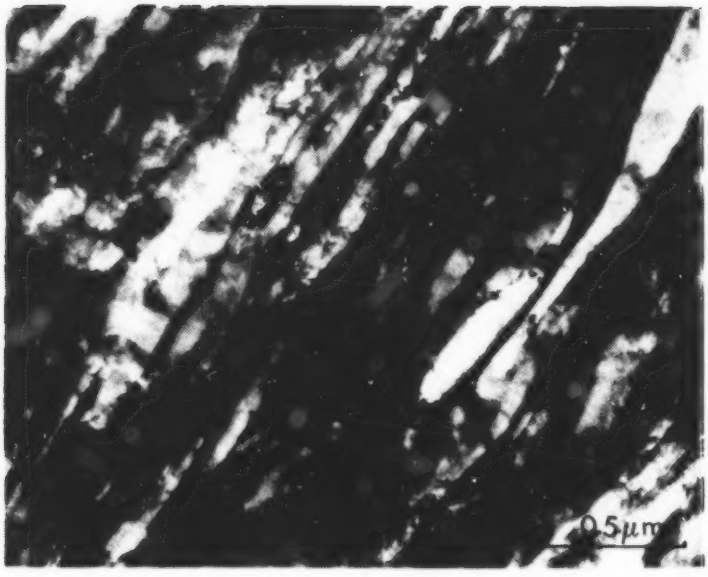

Figure 17c: Dark Etching Region, same as 17a, 75,000 × (Neg. 3245)

Figure 18: Macro Photo of K21 Flake (Neg. 7c)

Figure 19: Optical Micrograph of K21 Flake, 500 × (Neg. 12KF)

Figure 20: Sample K21, 75,000 × (Neg 3343)

Figure 21a: Sample K21, Another Area, 75,000 × (Neg. 3344)

Figure 21b: Diffraction Pattern Corresponding to Figure 21a (Neg. 3345)

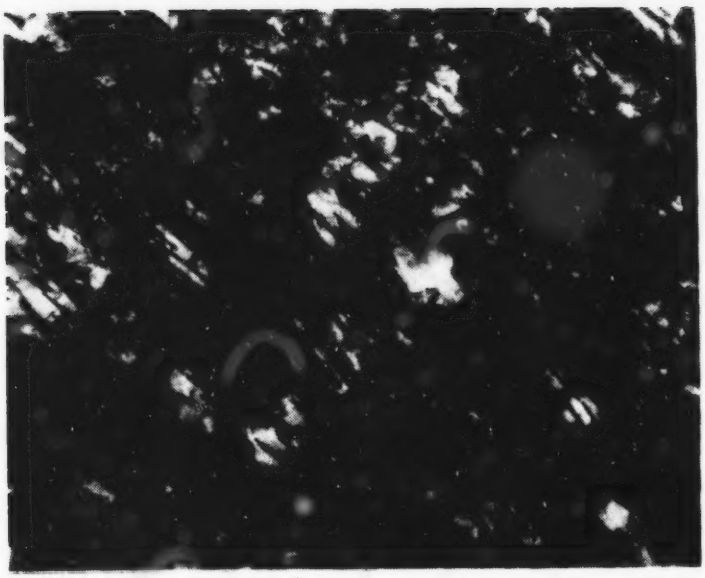

Figure 22: Sample K21, 25,000 × (Neg. 3347)

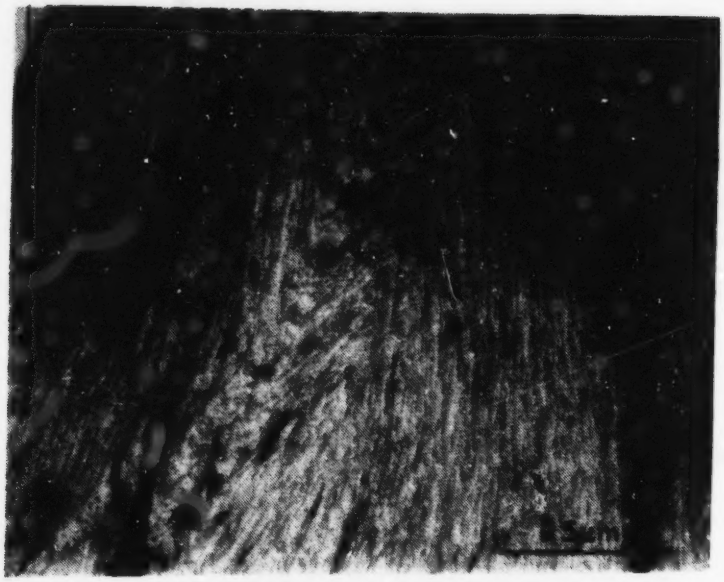

Figure 23: Optical Micrograph of K40P Flake, 500 × (Neg. 23KF)

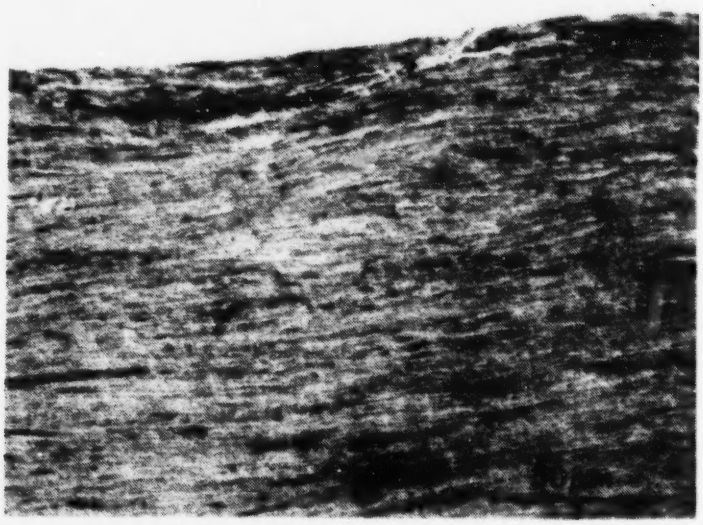

Figure 24: Optical Micrograph of K40P Flake, Another Area, 500 ×, (Neg. 24KF)

Figure 25a: Sample K40P, 75,000 × (Neg. 3156)

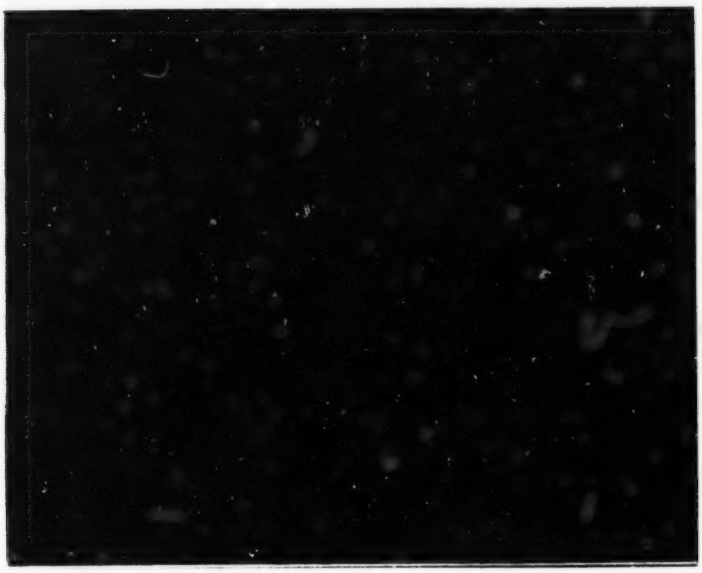

Figure 25b: Diffraction Pattern Corresponding to Figure 25a (Neg. 3153)

Figure 26a: Sample K40P, Another Area, 75,000 × (Neg. 3157)

Figure 26b: Diffraction Pattern Corresponding to Figure 26a (Neg. 3158)

REPORT DOCUMENTATION PAGE/PAGE DE DOCUMENTATION DE RAPPORT

REPORT/RAPPORT	REPORT/RAPPORT
1a TR-WE-46	NRC. NO. 24967 1b TDC TP 6939E
REPORT SECURITY CLASSIFICATION **CLASSIFICATION DE SÉCURITÉ DE RAPPORT** 2 UNCLASSIFIED	**DISTRIBUTION/DIFFUSION** 3 UNLIMITED

TITLE/SUBTITLE/TITRE/SOUS-TITRE (CLASSIFICATION) (UNCLASSIFIED)

4 ESTABLISHMENT OF QUANTITATIVE WEAR AND FATIGUE MODEL FOR RAILWAY RAIL SUBJECTED TO HEAVY TRAFFIC CONDITIONS AND DIFFERENT LUBRICATION REGIMES

AUTHOR(S)/AUTEUR(S)

5 Kalousek, J.; Fegredo, D.; Ghonem, H.; Laufer, E.E.; Steele, R.K.

SERIES/SÉRIE

6 Technical Report

CORPORATE AUTHOR/PERFORMING AGENCY/AUTEUR D'ENTREPRISE/AGENCE D'EXÉCUTION

7 National Research Council (Western Laboratory)
Division of Mechanical Engineering

SPONSORING AGENCY/AGENCE DE SUBVENTION

8 Transport Canada, Transportation Development Centre;
Association of American Railroads, Technical Research Center

DATE	FILE/DOSSIER	LAB. ORDER COMMANDE DU LAB.	PAGES	DIAGS	REFS
9 1985/05	10 3793-2-4	11 22200	12a 95	12b 52	12c 43

NOTES

13

DESCRIPTORS(KEY WORDS)/MOTS CLÉS

14 Rail Wear, Rail Lubrication, Rail Contact Fatigue, Rail Metallurgies: Bainite, Pearlite, Tempered Martensite, White Etching Layer

SUMMARY/SOMMAIRE

15 Wear rates and contact fatigue evaluation of several commercial and four types of experimental rail under three distinct lubrication regimes are reported. White etching layer present in rail flakes is examined.

ADDRESS/ADRESSE

16 Dr. C. Dayson (Head)
Western Laboratory
3904 West 4th Avenue
Vancouver, B.C. V6R 1P5 (604) 666-2623